Université de Montréal

Characterizing the Melanoma Brain Metastasis Microenvironment Using CyTOF IMC and the Adenosine Pathway in Melanoma

Par

Sarah Allard-Puscas

Département de Sciences biomédicales, Faculté de médecine

Mémoire présenté en vue de l'obtention du grade de Maître

en Sciences biomédicales, option science expérimentale

Avril, 2023

Université de Montréal

Département de Sciences biomédicales, Faculté de médecine

Ce mémoire intitulé

Characterizing the Melanoma Brain Metastasis Microenvironment Using CyTOF IMC and the Adenosine Pathway in Melanoma

Présenté par

Sarah Allard-Puscas

A été évalué par un jury composé des personnes suivantes

Gerardo Ferbeyre

Président-rapporteur

John Stagg

Directeur de recherche

Ian Watson

Codirecteur

Luke McCaffrey

Membre du jury

Résumé

Introduction: Le mélanome est le type de cancer de la peau le plus fréquent et les métastases du système nerveux central en sont une complication fréquente et grave. Les cellules de mélanome interagissent avec une grande variété de types de cellules dans le microenvironnement tumoral (MET), ce qui peut entraîner des effets pro- ou antitumoral. Plusieurs voies immunosuppressives ont été récemment découvertes comme des cibles médicamenteuses prometteuses, notamment la voie de l'adénosine. L'adénosine extracellulaire s'accumule dans le MET suite à l'hydrolyse de l'ATP par les ectonucléotidases CD39 et CD73. Les principaux régulateurs de la voie de l'adénosine sont CD39, CD73, et les récepteurs A2a et A2b.

Matériel et Méthodes: Pour caractériser spatialement le MET des métastases cérébrales du mélanome (MCM), nous avons quantifié l'expression de 35 marqueurs protéiques à l'aide du time of flight (CyTOF) Imaging Mass Cytometry (IMC) dans 21 MCM, et segmenté et classé plus de 130 000 cellules. Ensuite, pour évaluer les effets du ciblage du récepteur A2b et du CD73 dans la voie de l'adénosine sur le développement du mélanome, nous avons utilisé les tests de prolifération IncuCyte et MTS pour évaluer la prolifération des cellules de mélanome.

Résultats: Dans notre ensemble de données, les caractéristiques immunitaires du MET étaient hétérogènes dans tous les échantillons et le type de cellule le plus courant après les cellules cancéreuses du mélanome était les macrophages dérivés de la moelle osseuse (MDMO). Les échantillons à propagation leptoméningée avaient significativement moins de neutrophiles, de MDMO de type M1, d'autres cellules T et plus de cellules cancéreuses dans leur microenvironnement. Nous avons observé que la stimulation du récepteur A2b a un effet antiprolifératif sur les cellules cancéreuses du mélanome.

Conclusion: Cette recherche met en évidence le rôle du MET dans la progression du mélanome et l'importance du MET comme base pour le développement de nouvelles thérapies pour les patients atteints de cancer.

Mots-clés : Mélanome, Cancer, Métastase, Voie de l’adénosine, Microenvironnement Tumoral, CyTOF IMC, Récépteur A2b, CD39, CD73, Test de prolifération.

Abstract

Background: Melanoma is the most frequent type of skin cancer and metastasis to the central nervous system is a common and serious complication of it. Melanoma cells interact with a wide variety of cell types in the tumor microenvironment (TME) which can lead to tumor-promoting or tumor suppressive effects. Several immunosuppressive pathways have emerged as promising drug targets, including the adenosine pathway. The extracellular adenosine accumulates in the TME as the result of ATP hydrolysis by the ectonucleotidases CD39 and CD73. Key regulators of the adenosine pathway are CD39, CD73, A2a and A2b receptor.

Methods: To spatially characterize the TME of melanoma brain metastases (MBM), we quantified the expression of 35 protein markers using time of flight (CyTOF) Imaging Mass Cytometry (IMC) in 21 MBMs, and segmented and classified over 130 000 cells. Then, to evaluate the effects of targeting the A2b receptor and CD73 in the adenosine pathway on the development of melanoma, we used the IncuCyte and MTS proliferation assays to assess the proliferation of melanoma cells.

Results: In our dataset, the immune landscape of the TME was heterogeneous across all samples and the most common cell type after melanoma cancer cells were bone marrow derived macrophages (BMDM). Samples with leptomeningeal spread had significantly less neutrophils, M1-like BMDM, T other cells and more cancer cells in their microenvironment. We observed that stimulation of the A2b receptor has an antiproliferative effect on melanoma cancer cells.

Conclusion: This research highlights the role of the TME in the progression of melanoma and the importance of the TME as grounds for development of new therapies for cancer patients.

Keywords: Melanoma, Cancer, Metastasis, Adenosine Pathway, Tumor Microenvironment, CyTOF IMC, A2b receptor, CD39, CD73, Proliferation assay.

Table of contents

List of Tables

List of figures

List of abbreviations

TME = tumor microenvironment

INFγ = interferon-γ

IL-# = Interleukin-#

NK cell = Natural Killer cell

VEGF = Vascular Endothelial Growth Factor

GFAP = Glial Fibrillary Acidic Protein

BMDM = bone marrow-derived macrophages

CSD = cumulative solar damage

MBM = melanoma brain metastasis

ICI = immune checkpoint inhibitor

IMC = Imaging Mass Cytometry

CyTOF = Cytometry by Time of Flight

PLC = phospholipase C

IP3 = Inositol triphosphate

DAG = Diacylglycerol

NFkB = Nuclear factor kappa B

TNFα = Tumor necrosis factor α

VEGF = Vascular endothelial growth factor

VEGF-R = Vascular endothelial growth factor receptor

TMA = Tissue microarray

PCR = Polymerase Chain Reaction

FACS = Fluorescence-activated cell sorting

UMAP = Uniform Manifold Approximation and Projection

NMSC = Non-melanoma skin cancers

PD-1 = Programmed death-ligand 1

CTLA-4 = Cytotoxic T-lymphocyte-associated protein

DAPI = 4’,6-diamidino-2-phenylindole

MTS = 3-(4,5-dimethylthiazol-2-yl)-5-(3-carboxymethoxyphenyl)-2-(4-sulfophenyl)-2H-tetrazolium

Acknowledgments

I would like to thank my supervisors, Dr. John Stagg and Dr. Ian Watson for their guidance and mentorship throughout my graduate studies. Their expertise in the field has been fundamental and I am deeply grateful for their commitment to my success. I have learned lots from their mentorship and I feel privileged to have had the chance to work with them. Also, I would like to thank present and past members of John Stagg's lab: Isabelle Cousineau, Bertrand Allard, David Allard for their continuous support. I would also like to thank present and past members of Ian Watson's lab: LeeAnn Ramsay, Mathieu Lajoie for their bioinformatics expertise, Alexandra Lissouba, Vanessa Gaspar, Dan Moldoveanu, Jamie Magrill.

I would also like to thank all the other labs implicated in this project.

I would like to acknowledge funding from the Institut du Cancer de Montréal.

1. Chapter 1 – Introduction

1.1 Tumor Microenvironment

Over the last few years, multiple ground-breaking discoveries have shown that the tumor microenvironment (TME) plays a pivotal role in tumor development which has sparked the interest of multiple researchers across the world (1). Of upmost importance, the targeting of specific components of the TME could constitute the grounds for development of new therapies for cancer patients. The TME is composed of various elements such as stromal fibroblast cells, blood vessels, cancer cells, immune cells, and the extracellular matrix amongst others (2). Immune cell infiltration with cells like B cells, T cells, natural killer (NK) cells, macrophages, neutrophils, and dendritic cells, have been shown to be key players in the TME after extensive investigations (2). For example, in a study by Gentles et al. (2015) realized to evaluate the prognostic effect of the aforementioned cell types, they analyzed the link between overall survival and the immune infiltration of 5,782 tumors originating from 25 different types of cancer. The infiltration of the cells was analyzed using tissue microarray analysis, flow cytometry, and H&E staining of tumor tissue sections for morphological analysis. In their study, gamma delta T cells and CD8 T cells were associated with a favorable prognosis and macrophages were associated with an adverse prognosis (3).

One of the most abundant immune cell infiltrates in the TME of most tumors are macrophages. They are categorized into two subtypes: M1-like and M2-like (4). M1-like type macrophages, also called classically activated macrophages, have a tumor suppressive effect and mediate pro-inflammatory processes in the TME. M2-like type macrophages, also called alternative activated macrophages, have a tumor growth promoting effect and promote metastasis (4). However, recent studies show that using this dichotomic approach has its limitations and is an oversimplification of these cells, as macrophages can switch phenotypes in response to stimuli in the environment (5). This phenotype switch can be triggered by lipopolysaccharide and interferon-γ which stimulates macrophages into M1 phenotype, and cytokines such as IL-4 and IL-13 which stimulates macrophages into M2 phenotype (5). Additionally, it has been observed

that macrophages accumulate in tumors that underwent therapeutic treatments, such as chemotherapy, radiotherapy, or anti-VEGF therapy. This can lead to therapy resistance, but the exact mechanism is unknown (1).

Another abundant cell type in the TME are neutrophils, which are granulocytic cells. In tumors, the role of neutrophils is controversial. Some studies suggest that tumor associated neutrophils have an anti-tumoral effect and can inhibit metastasis (6-9). On the other hand, some studies have shown that tumor associated neutrophils have a pro-tumor effect by promoting angiogenesis and migration of cells (10-12). This controversy can be explained by the fact that neutrophils can switch phenotypes depending on the environment and undergo alternative activity. For instance, transforming growth factor-b in their environment can promote neutrophils to have pro-tumor properties whereas the presence of interferon-b or the inhibition of transforming growth factor-β can promote neutrophils to have anti-tumoral properties (13, 14). Also, it has been observed that in the peripheral blood, a high ratio of neutrophils to lymphocytes could be associated with poor survival in various cancers such as esophageal, lung, pancreatic, colorectal, and liver cancer (15). In a study by Gungabeesoon et al. (2023), they found that neutrophils that acquire interferon gene signature are essential for successful immunotherapy for lung cancer (16). This anti-tumor function of neutrophils was attributed to BATF3-dependent dendritic cells, IL-12 and INF-γ. They also found that following anti-PD-1 treatment, there was a neutrophil increase in the TME which led to activation of T cell mediated tumor killing near blood vessels in the tumor stroma (16). In a study by Ager (2023), it was found that anti-PD-1 treatment breaks tolerance of cancer cells and increases the effectiveness of the endogenous killer T-cell response (17).

1.2 Tumor microenvironment of brain metastasis

The TME of brain metastasis differs compared to its primary tumor. The central nervous system is composed of a relatively immune privileged environment because of the blood-brain barrier (18). The blood-brain barrier is made up of endothelial tight junctions which restricts the passage of blood borne cells and substances like ions and solutes. The tight junctions in the capillaries are

regulated by highly specialized proteins that are modulated via complex intra and extracellular signaling pathways. The presence of tissues-resident cell types, the extracellular matrix, and the blood-brain-barrier contribute to the differences in the microenvironment of the brain (18).

Astrocytes are glial cells and are the most abundant cell type in the brain, representing around 50% of all brain cells and they play a role in modulating synaptic activity (19). They are vital for homeostasis and provide support for other cells such as neurons and endothelial cells (5). In MBM, astrocytes play a role in tumor invasion by the release of heparinase, IL-23 and neutrophins (20-22). Glial Fibrillary Acidic Protein (GFAP) is commonly used as a marker to identify astrocytes but has limitations since it doesn't mark the cell population in its entirety (23). As explained by Nolte et al. (2001), GFAP mRNA can be produced in multiple cells, but it is not always transcribed. When GFAP is used in immunohistochemistry to mark astrocytes, only the intermediate filament cytoskeleton of mature astrocytes is labelled. Therefore, only regions of the brain that express intermediate filament protein will be labelled and not the rest thus limiting its use (24).

In brain tumors, macrophages represent the largest population of immune cells and up to 30% of the tumor mass (18). Several different populations of macrophages are found in the microenvironment of the brain such as tissue-resident microglia and bone marrow-derived macrophages (BMDM) (18). Microglia are sessile macrophages and play an important role in the innate immune system of the brain. Studies have shown that they can have tumor-suppressive functions as well as tumor-promoting functions (5). Circulating monocytes can be recruited to the brain in pathological conditions and give rise to BMDM. More research is needed to analyze if the role of resident microglia and BMDM are similar (18).

T cells are usually rare in the brain microenvironment but during pathologic conditions they can migrate to the brain (5). Depending on the T cell type, they can express a tumor-suppressive or tumor-promoting effect. Studies have shown that tumor-suppressive T cells are CD3 positive, cytotoxic CD8-positive and CD45RO-positive T cells, hence their presence in the brain microenvironment has been associated with a better overall survival. Tumor-promoting T cells are FoxP3-positive and PD1-positive T cells (5).

1.3 Melanoma

The most aggressive type of skin cancer which is responsible for the most skin cancer related deaths is melanoma. In Canada, melanomas represent 3.8% of all new cancers for men and 3.3% for women. It is estimated that one in 42 men and one in 52 women will develop melanoma during their lifetime (25). In the USA, it is estimated that melanoma of the skin represents 6% of all new cancers in men and 5% in women (26). According to the American Cancer Society, melanoma represents about 1% only of all skin cancers (27). In Canada, non-melanoma skin cancers (NMSC) represent 28% of all new cancers. Common NMSCs include basal cell carcinomas and squamous cell carcinomas which represent 77% and 23% respectively of all NMSCs (28). Melanomas however, despite not having the highest incidence rate, have the highest mortality of all skin cancers (26). According to the American Cancer Society cancer facts & figures 2022 analysis, the 5-year survival for all SEER stages combined is 93%. The 5-year survival rate by stage of diagnosis in the USA is 99% for local melanomas that are confined within the original site. For regional melanomas that invade surrounding tissues, or invades lymph nodes, or both, the survival rate drops to 68%. Distant melanomas, meaning the metastasis have spread to distant sites from the original site, have a 5-year survival rate of 30% (26). On the other hand, most NMSC can be cured especially if detected and treated early, with deaths related to them being uncommon in otherwise healthy individuals (26, 29). According to the Canadian Cancer Society, the 5-year survival rate for basal cell carcinomas is 100%, and 95% for squamous cell carcinomas (30).

Despite prevention campaigns, the incidence of melanoma has steadily increased throughout the years and is continuing to rise (31). In Canada, from 1984 to 2017, the incidence rate has increased by an average of 2.2% and 1.4% per year for male and female, respectively (32).

Table 1. WHO classification of melanoma.

Type	Description
Cumulative solar damage	High-CSD include lentigo maligna melanoma, desmoplastic melanoma
	Low-CSD include superficial spreading melanoma
Not associated with cumulative solar damage	Acral melanoma, mucosal melanoma, uveal melanoma, splitz melanoma, melanoma arising from congenital nevi or blue nevi
Nodular melanoma	Can occur in Cumulative solar damage or
	Not associated with cumulative solar damage

Melanoma arises from transformed melanocytes which are found in the basal layer of the epidermis of the skin. Their primary function is to protect the skin from ultraviolet radiation by producing melanin, which is responsible for the pigment of the skin, hair, and eyes. One of the major environmental risk factors for developing melanoma is the exposure to harmful ultraviolet radiation (33). Previously, melanoma was classified into anatomical subtypes based on the location of the primary tumor. The four main types of melanomas were superficial spreading, nodular, lentigo maligna and acral lentiginous (34). In 2018, the World Health Organization (WHO) revised its classification and melanoma is now classified into nine distinct subtypes based on histological, genomic, clinical, and epidemiologic characteristics (35). With this new classification, melanomas are first divided into three categories: those with cumulative solar damage (CSD), those not associated with cumulative solar damage, and nodular melanoma (Table 1). The cumulative solar damage category is then further divided into high and low cumulative solar damage according to the histopathologic degree of solar elastosis surrounding the melanoma. Melanomas with high-CSD include lentigo maligna melanoma and desmoplastic melanoma. Low-CSD types include superficial spreading melanoma. The “not associated with cumulative solar damage” category includes acral melanoma, mucosal melanoma, uveal melanoma, splitz melanoma, and melanoma arising from congenital nevi or blue nevi (34). Melanoma can metastasize to various organs such as liver, skin, lungs and brain (36).

1.4 Melanoma brain metastasis

The development of metastasis to the central nervous system is a common and serious complication of melanoma. Brain metastases occur most commonly in patients with lung cancer, breast cancer and melanoma, respectively (37). The exact incidence of MBM is uncertain but, in previous studies, it has been observed that around 50% of patients with stage IV melanoma develop brain metastasis. During autopsies, it has been discovered that around 80% of patients have central nervous system involvement (38, 39). Brain metastasis may arise in different parts of the brain such as the parenchyma, dura mater and leptomeninges (40). Historically, the overall survival for patients with MBM was very poor, with a median survival of approximately 4 months from metastasis diagnosis. However, with the development of systemic therapies, such as immune checkpoint inhibitors, survival rates have improved drastically, but still, not all patients respond favorably (38). New immunotherapies will be discussed later in the paper.

The TME of MBM has not yet been well-characterized and little is known about the specific immunologic components. One major challenge of targeting the MBM TME is to be able to differentiate pro-tumor cells and normal cells in order to avoid side effects of targeting normal healthy cells (1). An in-depth understating of the MBM TME is needed to develop drugs for therapeutic targeting of the MBM TME.

1.5 Leptomeningeal disease

A subset of patients with brain metastases have involvement of the leptomeninges and cerebrospinal fluid, known as leptomeningeal spread (41). Leptomeningeal disease, also known as neoplastic meningitis, is defined as the infiltration of tumor cells in the leptomeninges of the brain, spinal cord, and cerebrospinal fluid (42, 43). It is a late-stage complication of systemic cancers (41). Leptomeningeal disease is associated with rapid disease progression and a poor prognosis with an overall survival of 4-6 weeks without treatment and 3-5 months with treatment (41, 44). The leptomeninges are part of the meninges and includes the arachnoid and pia mater, with the cerebral spinal fluid being present between the two layers (41, 42). The three most

common tumors associated with a higher risk of developing leptomeningeal disease are breast cancer, lung cancer and melanoma, which occurs in 10-25%, 3-5% and 5% of patients respectively (45-47). The pathogenesis of leptomeningeal spread is not fully understood. Some studies have suggested that leptomeningeal spread occurs via hematogenous spread (48). Patients often presents with non-specific symptoms such as headaches, nausea, vomiting and cranial nerve palsies making leptomeningeal spread hard to diagnose, and resulting in a late-stage diagnosis (48).

1.6 Melanoma brain metastasis standard of care

The standard of care for metastatic brain melanoma is local treatment, either surgery or radiation (49). Surgery is used for symptomatic and large metastasis (49). Often, radiotherapy follows, to decrease risk of metastasis recurrence. There are different types of radiotherapy: stereotactic radiosurgery and whole-brain radiotherapy. Whole-brain radiotherapy is mostly used for palliative care (50). In a study by Hong et al. (2019), researchers have shown that whole-brain radiotherapy does not offer clinical benefit regarding distant intracranial control and survival (51). In addition, most patients also receive systemic treatments, such as chemotherapy, targeted therapy, or immunotherapy. However, existing treatments have significant limitations, and more work needs to be done to find more effective treatments.

1.7 Immunotherapy

Recent findings on the TME have led to the discoveries of novel targets and improvements of cancer therapies. This has been seen especially with immunotherapies that potentiate host antitumor immune responses. Immunotherapy is a new type of systemic treatment that has been proven to be effective in treating metastatic melanoma (52). There are different types of immunotherapies and one of the current therapies used in melanoma is immune checkpoint inhibitors (ICI). ICI inactivates checkpoint proteins on the surface of tumor cells and thus allow T

lymphocytes to perform their role of tumor suppression (53). An example of a checkpoint protein that is found on the surface of tumor cells is the Programmed death-ligand 1 protein (PD-1). PD-1 directly attenuates T cell receptor signaling by acting in a negative feedback loop. PD-1 thus acts as a negative signal to attenuate T cell response. Since immune checkpoint receptors can attenuate the T cell response that is needed to combat cancer, an ICI like anti-PD-1 can inhibit PD-1's actions and thus allow T cells to attack the tumor cells (54). Another ICI example is anti-CTLA-4 (anti-cytotoxic T-lymphocyte-associated protein) which is reported to have similar properties to PD-1 (54).

ICI combined with anti-PD-1 and anti-CTLA4 antibodies can produce a long-term durable response for around 50% of melanoma patients (53). Unfortunately, not all patients respond to this type of therapy. This is a reason why characterizing the tumor microenvironment of melanoma brain metastasis is important to better understand why some patients respond favorably to ICI while others do not.

1.8 Time-of-flight (CyTOF) Imaging Mass Cytometry (IMC)

Traditionally, conventional immunochemistry has been used in the field to characterize cell-cell interactions. However, immunochemistry is limited in terms of number of simultaneous fluorochromes that can be used, which is less than 10 at once, due to overlapping emission spectra (55). CyTOF IMC allows multiplexed analysis of up to 40 markers at a time for a given tissue section (56). CyTOF IMC technology is used to spatially map the TME and to better understand tumor-immune interactions with an unprecedented level of detail by combining principles of mass spectrometry and flow cytometry.

In order to discover factors indicative of positive prognostic in immunotherapy treatments of metastatic melanoma, Martinez-Morilla et al. (2021) used IMC to quantitatively measure 25 markers simultaneously. They have successfully identified a series of biomarkers in the TME and the stroma that are associated with a better response to immunotherapy such as MHC-I, B2M, CD8 and LAG3 amongst others (57). CyTOF IMC technology has been used successfully in multiple

studies to characterize cell-cell interactions in melanoma TME. In a study by Moldoveanu et al. (2022), CyTOF IMC was used to spatially map the TME of melanoma patients (58). They used 35 simultaneous markers and profiled over 220 000 individual cells where they were able to identify and spatially characterize interactions between melanoma cells, lymphocytes, macrophages, and stromal cell populations. They found that proximity of antigen-experience cytotoxic T cells to melanoma cells were associated with a favorable response to ICI therapy. With the help of multiplex single-cell technology, the spatial cell-cell interactions within the TME were quantified and underlines the potential of CyTOF IMC in understanding immune responses. In a study by Tantalo et al. (2021), CyTOF IMC was successfully used to describe description of melanoma tumor-infiltrating lymphocytes at a greater depth than would otherwise have been possible with conventional techniques. This allowed them to detail the activation status, functional polarization and analyze a variety of cellular parameters (59). In a study by Karimi et al. (2023), they used CyTOF IMC to characterize 1.1 million cells of high-grade melanomas and brain metastasis tumors and successfully described key elements in the TME associated with a better survival in patients (60). Amongst others, these studies highlight the potential of CyTOF IMC as an effective tool to quantify and characterize the TME in melanoma patients.

1.9 The adenosine pathway

The adenosine pathway is considered a key immune checkpoint in tumor immunity and could potentially become a new drug target for melanoma patients. In different cancer types, it has been found that adenosine has roles in the pathological process of cell proliferation, angiogenesis, cell growth, apoptosis, and immune responses (61, 62). Adenosine is a purine nucleoside, and it is produced in the intracellular and extracellular environment. Intracellularly, adenosine is produced from AMP hydrolysis by either intracellular 5'-nucleotidase or S-adenosylhomocysteine (63, 64). Extracellular adenosine is mainly regulated by enzymes such as CD39 and CD73, which respectively degrade ATP into ADP and AMP, and AMP into adenosine (Figure 1) (65). The extracellular adenosine produced by CD39 and CD73 interacts with four G-protein-coupled receptors: A1, A2a, A2b and A3 (63, 66).

These adenosine receptors are found on various cell types, including melanoma cancer cells, and their effect is concentration dependent (67, 68). They are also found on various immune cells that have a crucial role in cancer pathogenesis such as macrophages, myeloid-derived suppressor cells, NK cells, dendritic cells, T cells, regulatory T cells and others (68). A1 and A3 receptors are of the Gi/0 type. The Gi type inhibits adenylate cyclase activity causing a decrease in cAMP production which leads to inhibition of protein kinase A (PKA). The G0 activity activates phospholipase-C (PLC) which leads to the production of inositol-tri-phosphate (IP3) and diacyl-glycerol (DAG) (69). A2a and A2b are of the Gs type, activate adenylate cyclase and increase AMP thus activating PKA and increasing IP3 and DAG (70, 71). A2b and A3 receptors can also activate Gq type proteins and activate phospholipase C which will increase cAMP (72).

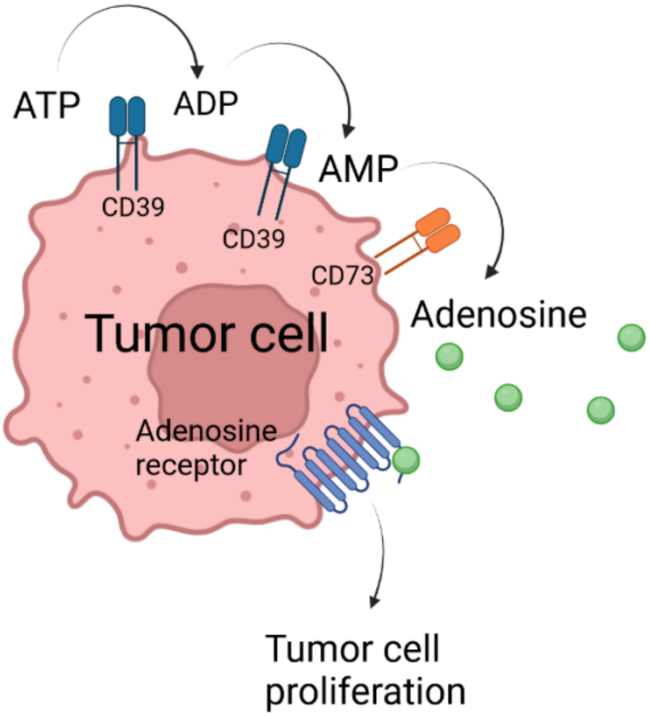

Figure 1. The adenosine pathway. In the microenvironment of the tumor, the extracellular adenosine accumulates as the result of ATP hydrolysis by the ectonucleotides CD39, CD73. The adenosine pathway is regulated by CD39, CD73 and the activation of the A2b receptor. CD39 transforms ATP into ADP and AMP. CD73 transforms AMP into Adenosine. Adenosine binds to its receptors A1, A2b, A2a and A3.

1.9.1 The role of the adenosine pathway in cancer pathology

A study by Dastjerdi et al. (2016) found that A1 adenosine receptor stimulation by agonists dramatically decreases cancer cell apoptosis via the downregulation of p53 and caspases 3, 8 and 9 in MCF-7 breast cancer cells (73, 74).

Activation of the A2a adenosine receptors leads to immunosuppression via the inhibition of nuclear factor kappa B (NFkB), T cell receptor (TCR) and JAK-STAT signaling pathways (75). In a study by Ohta et al. (2006), it was shown that A2a receptor activation protects tumors from anti-tumor T cells (76). This immunosuppressive effect is known to be a hallmark of cancer and to promote cancer progression (76). However, in a study by Merighi et al. (2002), it was found that A2a can also mediate melanoma cell death in humans (77).

The A2b adenosine receptor is known to have a role in the pathogenesis of human cancer and has functions in metastasis and tumor progression (78). In a study by Stagg et al. (2010), it was found that activation of A2b adenosine receptor promoted spontaneous lung metastasis of breast cancer (79). In a study by Mittal et al. (2016), it was found that the addition of an A2b adenosine receptor inhibitor decreased metastasis (80). This pro-metastatic activity was found via A2b knocked down mice where metastases were reduced compared to the mice with a functioning A2b receptor. They also found that in tripe-negative breast cancer cell lines, a higher expression of A2b adenosine receptors is associated with promotion of tumor metastasis and thus a worse prognosis (80). In a study on oral squamous cell carcinoma by Kasama et al. (2015), it was found that the A2b receptor is upregulated when compared to normal oral keratinocytes (81). When they knocked down the A2b receptor, they saw a significantly higher inhibition of cellular proliferation via hypoxia inducible factor 1 alpha (HIF-1 alpha) activation thus highlighting the pro-tumoral effect of A2b (81). Similar results suggesting A2b's tumor cell proliferation effects has been found by other studies as well in colon cancer (82), prostate cancer (83, 84), and bladder cancer (85).

Conversely, some studies suggest that A2b adenosine receptor activation may have anti-tumoral effects via it's ligand-independent anti-inflammatory effects (78). In a study by Sun et al. (2012),

they suggest that this paradoxical function of anti-tumoral and anti-inflammatory functions might stem from interactions with ligand-independent molecules like the p105 subunit of NFkB with the A2b adenosine receptor (86). They found that the binding of the p105 subunit to the C-terminal of the A2b receptor inhibits NFkB activation and led to a decrease in IL-10, increase in IL-12 and tumor necrosis factor (TNFα). In melanoma specifically, it has been found that IL-10 expression by primary tumor cells is correlated with melanoma progression and metastasis (87). In a study by Yue et al. (1999), it was found that IL-12 directly up-regulated the expression of HLA class I and II and ICAM-1 on human melanoma cells resulting in an increased immunogenicity (88). In regards to TNF-alpha, this molecule can have both pro-tumoral and anti-tumoral effects in melanoma (89). In other studies, adenosine deaminase has been found to promote T cell activation via the interaction of CD26 and the A2b adenosine receptor (90). These opposing functions of the A2b adenosine receptor require deeper investigation to elucidate the conditions and molecules necessary for the different functions of this receptor.

In breast cancer stem cells and renal cancer cells, it's been found that activation of the A3 adenosine receptor by CI-IB-MECA will inhibit cell growth and cause apoptosis via the inhibition of ERK1 and ERK2 protein kinases (91-93). In a study by Kanno et al. (2012), it was found that addition of adenosine to human bladder cancer cell lines caused cell apoptosis via the upregulation of AIF expression by the A3 receptor mediated Gq protein and PKC pathway (94). They also found that A3 receptor knocked-down mice and addition of A3 adenosine receptor inhibitor causes increased cell growth compared to mice with a normal functioning A3 adenosine receptor (94).

1.9.2 The importance of the adenosine pathway in melanoma

It has been shown that tumors have more CD39 and CD73 in their microenvironment because of tissue hypoxia which results in the accumulation of adenosine in the TME (95). Adenosine can have both anti-tumoral and pro-tumoral effects depending on which adenosine receptor is

activated (77, 96). There are multiple studies that focus on the adenosine pathway as a potential target in multiple cancers, including melanoma (97-100).

In a study by Young et al. (2017) on patients with American Joint Committee on Cancer (AJCC) stage III melanoma, it was found that CD73 expression was correlated directly with patients presenting with nodal metastatic melanoma (100). Multiple studies have found an association between CD73 and a worst prognostic with reduced response to therapeutics (101-104). In a study by Reinhardt et al. (2017), they found that induction of CD73 is linked to melanoma phenotype switching to an invasive phenotype (105). This phenotype switching was secondary to immunosuppressive adenosine secretion caused by CD73 activation which led to the activation of the c-Jun/AP-1 transcription factor complex. Presence of CD73 can be used as a marker for nascent activation of the EMT-like invasive melanoma phenotype (105).

Activation of the A1 adenosine receptor will stimulate chemotaxis and motility of melanoma cells. Its activation will also increase expression of pro-angiogenic factors like vascular endothelial growth factor receptor (VEGF-R) and stimulate macrophage tumor infiltration (106). Activation of A2a receptors will inhibit tumor growth by decreasing cell viability and inhibition of cell clone formation in melanoma cells. Via PKC and MAPK, it will also increase cell proliferation (77). In a study by Sorrentino et al. (2015), it was found that activation of A2b receptors will increase tumor VGEF-A production and tumor growth (107). They used Bay60-6583 as a selective agonist for A2b adenosine receptors and found a significantly increased tumor VGEF-A expression, vessel density and accelerated tumor growth. They also blocked the A2b receptor with PSB1115 which resulted in a significant decrease in tumor growth via the inhibition of tumor angiogenesis and increasing T cell numbers in the TME (107). Similar results have been found in other studies (108). A3 receptor activation will inhibit melanoma growth. It increases melanin expression and DOPA oxidase activity in melanoma cells. Finally, A3 also causes Ang-2 accumulation and increases HIF-1 alpha expression (109).

2. Chapter 2 – Hypothesis and specific aims

Despite recent research efforts, little is known about the specific immunologic components of the tumor microenvironment of melanoma brain metastasis which is needed to later develop novel therapeutic avenues. The first aim of this thesis was to characterize and describe the microenvironment of MBM using imaging mass cytometry technology and optimize antibodies of the adenosine pathway (CD73 and A2a) for CyTOF IMC. Additionally, the adenosine pathway has been found to be a key immune checkpoint in tumor immunity in multiple cancer types. Our second aim was to examine the effectiveness of targeting specific components of the adenosine pathway on the development of melanoma. Specifically, to determine if the A2b receptor and CD73 have a proliferative effect in melanoma cancer cells. We hypothesize that A2b receptor and CD73 have a pro-proliferative effect in melanoma cancer cells. A deeper understanding of the adenosine pathway could potentially lead to new drug targets for melanoma patients.

3. Chapter 3 – Materials and Methods

3.1 Aim 1

3.1.1 Sample procurement

A cohort of 21 patients underwent surgical resection of melanoma brain metastasis from 2009 to 2019. The brain metastasis samples were procured from the tumor core or the tumor margin from the McGill University Health Center (MUHC) biobank following ethical approval. The clinical data was obtained from pathological and surgical reports for all patients. Clinical information was de-identified to respect confidentiality.

3.1.2 Immunostaining and IMC acquisition

The first step is designing a tissue microarray (TMA) slide. Immunostaining for all slides was performed by an affiliated laboratory (protocol on request). The panel was developed in collaboration with an affiliated laboratory. The panel was created to be able to characterize the melanoma brain microenvironment. The panel includes, lymphoid lineage markers, myeloid lineage markers, compartment markers and functional markers. Afterwards, the TMA is stained with a panel of 35 antibodies previously conjugated with heavy metal isotopes. The complete list and details of individual antibodies used in the panel can be found in supplementary table S1. All the antibodies used in this panel were previously validated to confirm specific binding and adequate staining. The TMA slide is then inserted into the CyTOF machine, and a laser ablates the tissue sample one micrometer square at a time (Figure 2A). This creates an ionized isotope plume that is picked up by a mass cytometer. This gives us the counts for the number of isotopes present in each image. Each image generated corresponds to one marker. IMC Data was acquired using the Hyperion Imaging System (Fluidigm). A total of 48 images were acquired.

A)

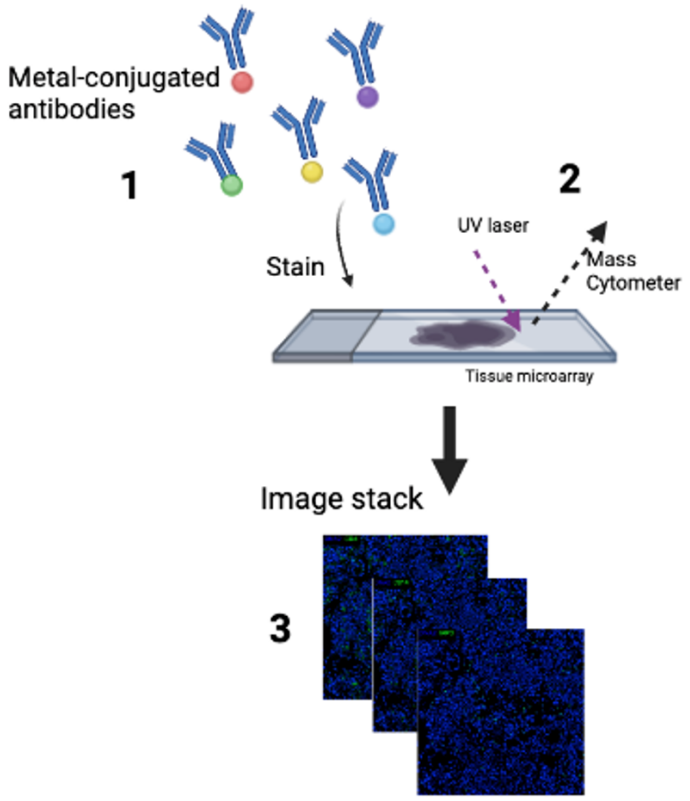

B)

Cells	Markers
Cancer	PMEL + and/or MelanA+ and/or PAnCK +
B cells	CD20+
Neutrophils	MPO+
Natrual Killer	CD94+
Dendritic cell	CD11c and HLA-DR+
Endothelial	CD31+
Astrocytes	GFAP+
Tc	CD3+/CD8+
Th	CD3+/CD4+/Foxp3-
Treg	CD3+ CD4+ Foxp3+
T other	CD3+, CD8-,CD4-
M1-like BMDM	CD68+/CD163-/P2Y12-
M2-like BMDM	CD68+/CD163+/P2Y12-
M1-like MG	CD68+/CD163-/P2Y12+
M2-like MG	CD68+/CD163+/P2Y12+
Cl Mo	CD14+/CD16-
Non-Cl Mo	CD14-/CD16+
Int Monocyte	CD14+/CD16+
Others	All -

Figure 2. Multiplex CyTOF IMC used to characterize the melanoma brain metastasis microenvironment. A) Illustration of the CyTOF IMC workflow used in our study: (1) TMA was stained with 35 antibodies that were previously conjugated with heavy metal isotopes (2) Tissue slides were then laser-ablated 1 μm^2 at a time in order to create an ionized isotope plumes that is then analysed by the mass cytometer. (3) Each image in the stack corresponds to one antibody marker and together it creates a 35-layer image-stack. B) List of markers that define the 19 cell types.

3.1.3 Cell segmentation and cell type classification

Cell segmentation was done using a computer algorithm that automates the detection of cells. This algorithm was developed by an affiliated laboratory (protocol on request) (60, 110).

To classify our cells (figure 3A), we first started with a marker for cancer which included cells that were positive for PMEL, MelanA and /or PanCK. After, CD68+ cells were used to define microglia and macrophages. P2Y12 was used to distinguish microglia (MG) and bone marrow-derived macrophages cells (BMDM). If cells were positive for P2Y12 and positive for CD163, they were classified as M2-like MG. If cells were positive for P2Y12 and negative for CD163, they were classified as M1-like MG. Cells that were negative for P2Y12 and positive for CD163 were classified as M2-like BMDM. If cells were P2Y12 and CD163 negative, they were classified as M1-like BMDM. After, cell that were negative for CD68 were further classified. Cells that were positive for CD3 were classified into T cells. Cells that were positive for CD8 were classified Tc. Cells that were negative for CD8, positive for CD4 and positive for FoxP3 became regulatory T cell (Treg). Cells that were negative for CD8, positive for CD4 and FoxP3 negative became T helper cell (Th). Cells that were CD8 negative, CD4 negative became T other. Cells that were CD20 positive became B cells. MPO positive cells became neutrophils. CD94 positive cells became NK cells. Cells that were CD16 and/or CD14 positive were classified into Monocytes. Monocytes were than subdivided into Cl monocytes (CD14 positive, CD16 negative), Int Monocytes (CD13 positive, CD16 positive) and non-Cl Monocyte (CD14 negative, CD16 positive). CD11c and HLA-DR positive cell were classified into dendritic cells.CD31 positive cells became endothelial cells. CD115 positive cells became mast cells. GFAP positive cells became astrocytes. Cells that did not express any of markers or lacked signal were classified as others (figure 3A). Finally, CD117 was included to identify mast cells. However, this gene is known to be amplified in melanoma cells, hence, it was not possible to use this marker to identify mast cells in the melanoma samples. Mast cells could have been CD117+ cells and melanoma negative therefore, we have decided to exclude this cell type from our analysis to avoid signal overlap and have added the cells to the “other” cell type.

3.1.4 Cell presence-absence analysis

For every cell type, we determined the presence or absence using a threshold of 20 cells per sample. The cell type was considered “present”, if the cell type contained at least 20 cells and

the cell type was considered “absent” if the number of cells was below the threshold of 20. A threshold of 20 cells per sample was used based of our lab’s previous findings (58).

3.1.5 Survival analysis

We performed 3 survival analyses. First, we compared survival between sex (female and male). Secondly, we compared survival between age groups (under 60 years old and over 60 years old). Thirdly, we compared survival between leptomeningeal spread status (with leptomeningeal spread and without leptomeningeal spread). Kaplan-Meier curves were plotted in R. P values were calculated using a log-rank test. Time zero was defined as date of surgery.

3.1.6 Comparison between different groups

When comparing core and margin samples we either compared the patients with cores only against the margin samples (all patients only appear once in the test) or compared cores and margin samples of the 5 patients that have both by doing a paired t-test.

When comparing leptomeningeal spread status, we either compared the patients with cores only by measuring the total number for each cell type across all samples or compared only margin samples. When patients had multiple cores, the median value was calculated for spatial comparisons.

When comparing alive and deceased patients we either compared the patients with cores only by measuring the median number for each cell type or compare only margin samples. When patients had multiple cores, the median value was calculated.

3.1.7 Spatial analysis

Delaunay triangulation was used to identify cells that are most likely in contact with each other. We used this method because the distance between the nucleus of cells varies depending on

their size. To represent cell-cell interactions, direct contact between cells were represented using edges and vertices for cells.

A shuffling algorithm (111, 112) and assortativity index (113) were used to map cell interactions while accounting for different contact frequencies between cell types and cell type proportions. The shuffling algorithm method was initially described by Denis Schapiro et al. (2017) (112).

Using the nominal assortativity formula, the assortativity coefficient was calculated for each cell type relative to the other cell types. Assortativity is defined as the tendency of cells to associate with a cell of the same type. A perfect associative mixing, when cells tend to touch cells of the same type, was attributed a positive value of 1. Perfect dissortative mixing, when cells tend to touch different cell types, was attributed a negative value of -1. A random mixing, when cells touch any type of cells, was attributed a value of 0.

3.1.8 Optimisation of CD73 and A2a antibody with immunofluorescence

The tissue microarrays (TMAs) were composed of ovarian and prostate cancer. Briefly, slides were first deparaffinized, then rehydrated. The slides were than demasked using a citrate buffer. Then slides were blocked with a protein blocking solution and incubated for 1 hour at room temperature. Primary antibodies were added to the slides and incubated overnight at 4°C. Secondary antibodies were added and incubated for 2 hours at room temperature. All antibodies are listed in supplementary table S2. After, DAPI was added for 10 minutes to the slides and thereafter were verticality dried at room temperature. Finally, slides were mounted using Prolong gold. The slides were imaged using VS-110 slide scanner and then were imported into Visiomorph DP for visualization. To differentiate background noise from a positive signal, we used a positive control (A2a cell pellet) and a negative control (TMA of colon and liver cells).

3.2 Aim 2

3.2.1 Cell line procurement

SK28 melanoma cells were obtained from the laboratory of Dr Simon Turcotte, Melanoma cancer cell lines were cultured in DMEM/F12 (SK23mel was cultured in RPMI) with addition of 10% FBS

NEAA Glutamax. All cells tested negative for mycoplasma using the Lonza MycoAlert mycoplasma detection kit.

3.2.2 Quantitative PCR

Quantitative PCR was used to determine which of the melanoma cell lines express A2b receptor. We used the RNeasy Mini Kit (Qiagen) to extract RNA from cell pellets of 17 melanoma cell lines by following the manufacturer's instructions and quantified on a Naondrop spectrometer (Thermo Scientific). First, RNA was reverse transcribed by using qScript cDNA Supermix (Quanta Biosciences). After, qPCR was performed and analyses with StepOne software V.2.3 were made. For every cell line, the reaction was performed in triplicates and the relative expression was normalized. The control for all cell lines was Tbp.

3.2.3 Fluorescence-activated cell sorting (FACS)

FACS was used to determine the expression of CD73 on SK28 cell line. Briefly, cells were harvested and added to FACS tubes. FACS buffer and FC block were added. After, cells were incubated for 10 minutes at 4℃. CD73 Antibody was added and then cells were incubated for 1 hour at 4 ℃. Tubes were then analyzed by the FACS machine, and the data was examined with FlowJo software.

3.2.4 Proliferation assay: IncuCyte and MTS on SK28 cell line

We first performed an IncuCyte. Briefly, SK28 cells were harvested and then trypsinized for 5 minutes at 37 ^{O} C. After, trypsin was inactivated using the cell culture media (DMEM/F12). Cells were then counted and were plated on a 96 well plate in quadruplicates in media. CD73 antibody was then added.

After, an MTS was performed on the SK28 cell line. Briefly, SK28 cells were harvested and then trypsinized for 5 minutes at 37 ^{O} C. After, trypsin was inactivated using the medium cell culture media. Cells were then counted and were plated on a 96 well plate at cells per well in quadruplicates in media. Plates were incubated for 72 hours, and Cell Titer 96 Aqueous Cell Proliferation Assay was used following the manufacture's protocol to determine cell viability.

4. Chapter 4 – Results

4.1 Aim 1

4.1.1 Clinical data summary of patients included in the analysis

The clinical data information (Table 2) for the 21 patients was obtained from the patient's electronic medical records (EMR) from the MUHC. For the patient demographics, 15 patients are male and 6 are female. Regarding the melanoma histological subtype, 11 had cutaneous melanoma, 2 had mucosal melanoma, 7 were unknown, meaning they were never diagnosed with melanoma and 1 was NA, meaning the information was not available on the EMR.

Regarding the age of the initial melanoma diagnosis, 9 were diagnosed before the age of 60 years old, 6 after the age of 60 years old and 6 were unknown. Regarding the melanoma brain metastasis diagnosis, 13 were diagnosed before 60 years of age and 8 were diagnosed after 60 years of age. 18 patients are deceased, 10 were under 60 years of age and 8 were over 60 years of age, and 3 patients are still alive to this date.

Regarding the treatment information, most of the patient got multiple types of treatments: radiotherapy and systemic treatment, such as immunotherapy, targeted therapy, chemotherapy. Regarding their last systemic treatment (Table 2), 10 patients received immunotherapy, 3 received targeted therapy, 3 received chemotherapy, 1 received anti-cancer agent, 1 patient was NA, and 3 received no systemic treatment. Regarding the response to the last treatment, 7 were classified as progressive disease, 4 as stable disease, 1 complete response and 9 NA. The response classification was obtained using the RECIST criteria (114).

In our data set, 15 tumor cores samples were obtained from patients, 1 tumor margin and 5 had a match tumor core and margin. Nine patients were diagnosed with leptomeningeal disease and 12 did not.

Table 2. Clinical data summary of the 21 patients included in the analyses.

		# patients	# images
Sex	Male	15	36
	Female	6	12
Melanoma histological Subtype	Cutaneous	11	24
	Mucosal	2	8
	Unknown	7	15
	NA	1	1
Age brain mets Diagnosis	Unknown	6	13
	Under 60	13	30
	Over 60	8	18
Age Death	Under 60	10	21
	Over 60	8	17
	NA (still alive)	3	10
Deceased	Alive	3	10
	Deceased	18	38
Last Systemic Treatment	Immunotherapy	10	29
	Targated therapy	3	4
	Chemotherapy	3	5
	Anti cancer agent	1	1
	NA	1	2
	No systemic treatment	3	7
Response to the last treatment	Progressive disease	7	17
	Stable disease	4	11
	Complete response	1	3
	NA	9	17
Biopsy	Pre treatment	9	17
	Post treatment	8	18
	Pre and Post	2	2 pre/ 1 post 3 pre/2 post
	NA	1	3
Tumor region	Core	15	28
	Margin	1	1
	Match core + margin	5	14 C /5 M
	Total # Core	-	42
	Total # Margin	-	6
Leptomeningeal disease	Yes	9	23
	No	12	25

4.1.2 CyTOF IMC panel used to characterize the melanoma brain metastasis microenvironment

DNA1, PMEL, MelanA and PAnCK all stained melanoma cells and were often co-expressed (Figure 3 A). A co-expression of CD68 and CD14 was observed. These are both expressed on macrophages (Figure 3B).

4.1.3 Analysis pipeline used to define the immune landscape of melanoma brain metastasis microenvironment

To better visualize the melanoma brain metastasis microenvironment, raw IMC images were converted into single-cell images. The cells were first segmented to identify where the cells were located in the images. Afterwards, cells were classified into 19 cell types (Figure 2B). The only marker that had an aberrant expression pattern was mast cells with a high expression of PMEL. We have decided to include this cell type into the "others" cell type. To assess the quality of our classification, a heatmap of the mean intensity of each marker for each cell type was generated (Figure 3C). For every marker in our data set, the highest intensity of each marker corresponded to the expression pattern that was expected.

Uniform Manifold Approximation and Projection (UMAP) dimensionality reduction was performed to confirm clusters reflecting the expression of our 19 markers (Figure 3D, supplementary figure S1). Distinct clustering patterns can be observed. CD68 + cells, which are M1-like BMDM, M2-like BMDM M1-like MG and M2-like MG, cluster together in the middle. Also, melanoma cell cluster together. When comparing the raw image with the segmented/classified image, similar staining patterns were observed (Figure 3E).

4.1.4 Immune infiltration analysis

After classifying each cell into its respective subtype, we looked at the general composition of our melanoma brain samples. Cancer cells were the most frequent type of cell, followed by "other" cell type and macrophages, M1-like BMDM and M2-like BMDM (Figure 4A, Supplementary Figure S2A). In our data set, T reg cells were the least present cell type. When looking at the immune composition of each individual samples, we can observe a higher amount of variation from samples that have a lot of immune infiltrates when compared to samples that do not have a lot of infiltration (Figure 4B, Supplementary Figure S2B). Most samples had M1-like BMDM present in their microenvironment but almost no samples had Treg in their microenvironment (Figure 4C, Figure 4D, Supplementary Figure S2C).

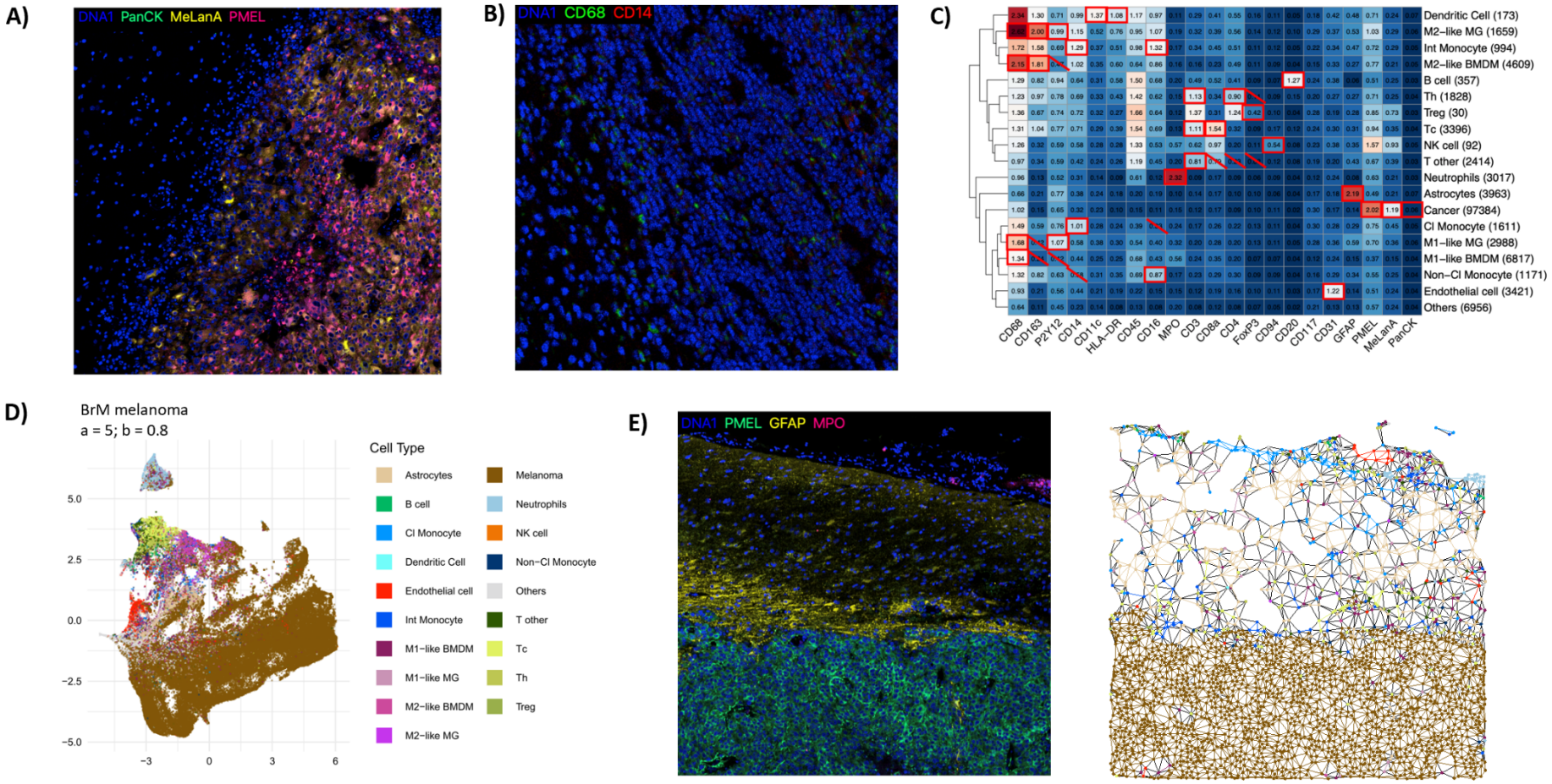

Figure 3. Analysis of melanoma brain metastasis microenvironment. A) Image illustrating the overlay of DNA1, PanCK, MelanA, and PMEL. B) Image illustrating the overlay of DNA1, CD68 (macrophage marker), CD14 (macrophage marker). C) Heatmap of the mean intensity of each identity marker for each cell type. The mean intensity is calculated per cell type from the normalized mean expression per cell. The red squares correspond to the marker the cell type should express. The red cross corresponds to the marker the cell type should not express. D) UMAP projection of all. Cells are labeled according to the classification. E) Example of raw image (left) and processed spatial graph with cell types labeled (right).

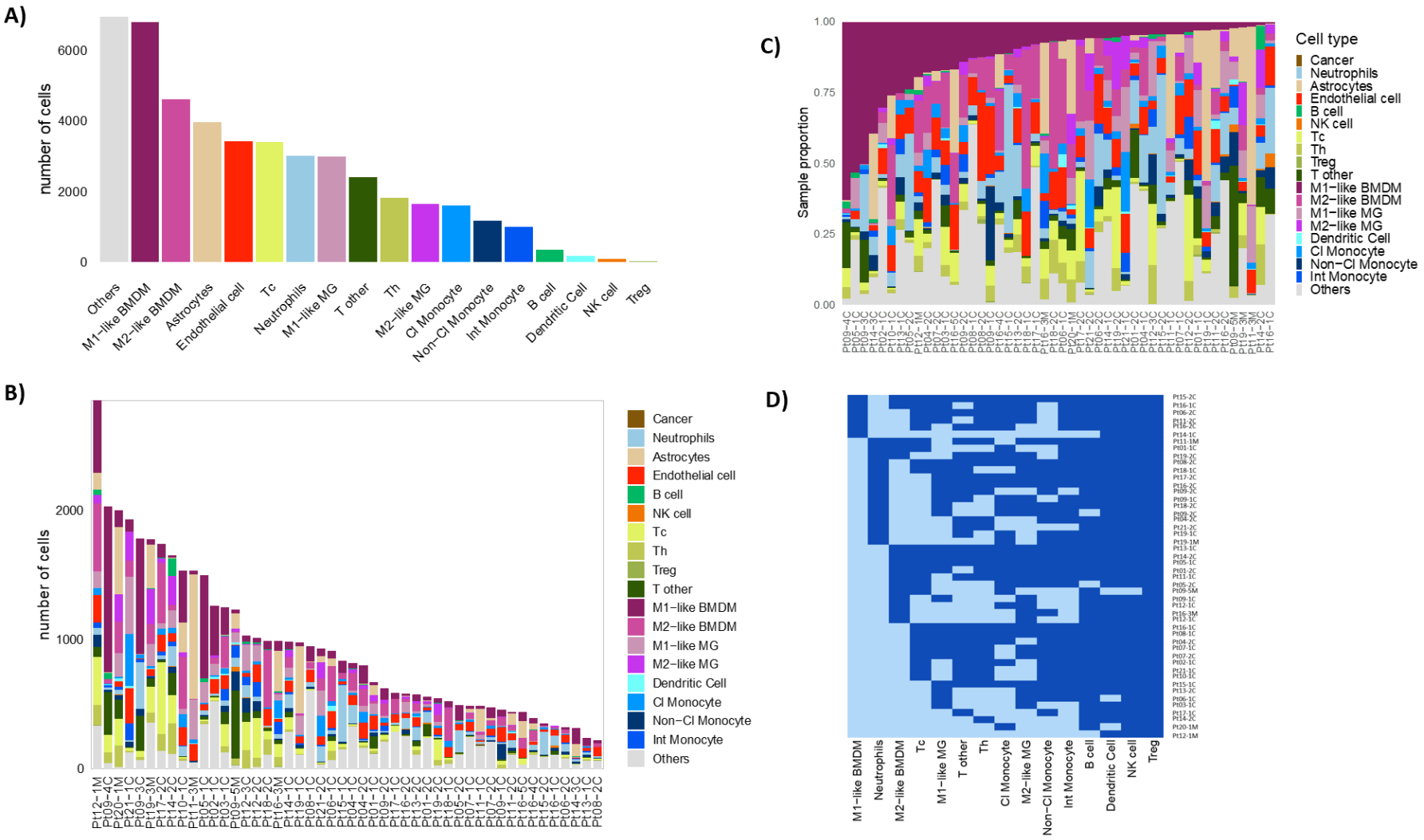

Figure 4. Immune infiltration analyses excluding cancer cells to allow better visualisation of other cell types. A) Total number of cells identified for each cell type. B) Total number of cells identified for each cell type for each patient. C) Stacked bar plot showing the proportion of all the different cell types in every sample ordered by increasing proportion of M1-like BMDM. D) Presence and absence of cell types in each sample. Light blue it is defined as at least 20 cells per lineage. Dark blue it is defined as less than 20 cells per lineage.

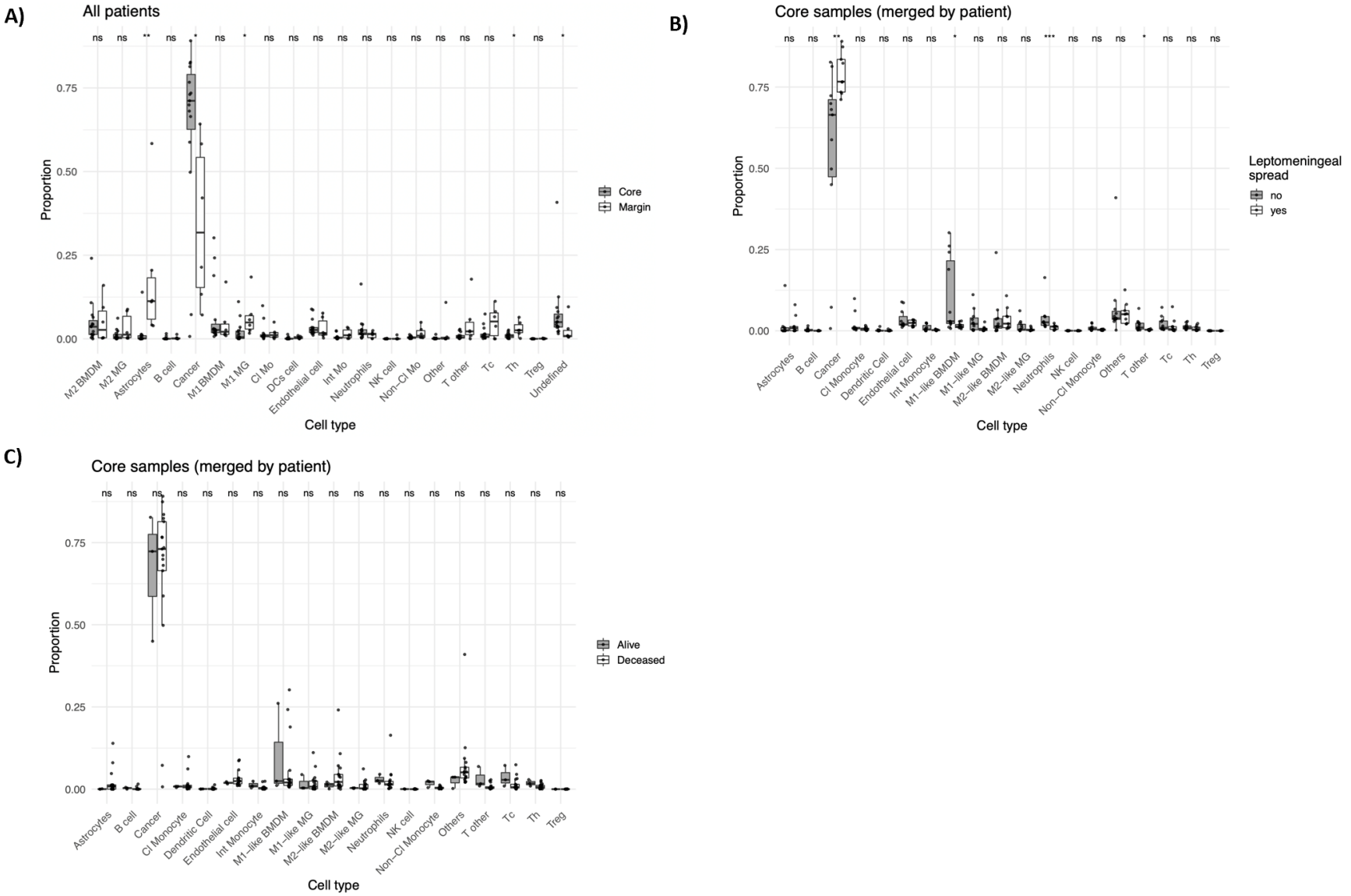

Figure 5. Cell type proportion comparisons. Boxplot showing distribution of cell types of proportions in every sample by comparing A) cores and margins where cores from the same patient have been merged, B) patients with or without leptomeningeal spread (core samples only), and C) alive and deceased patients.

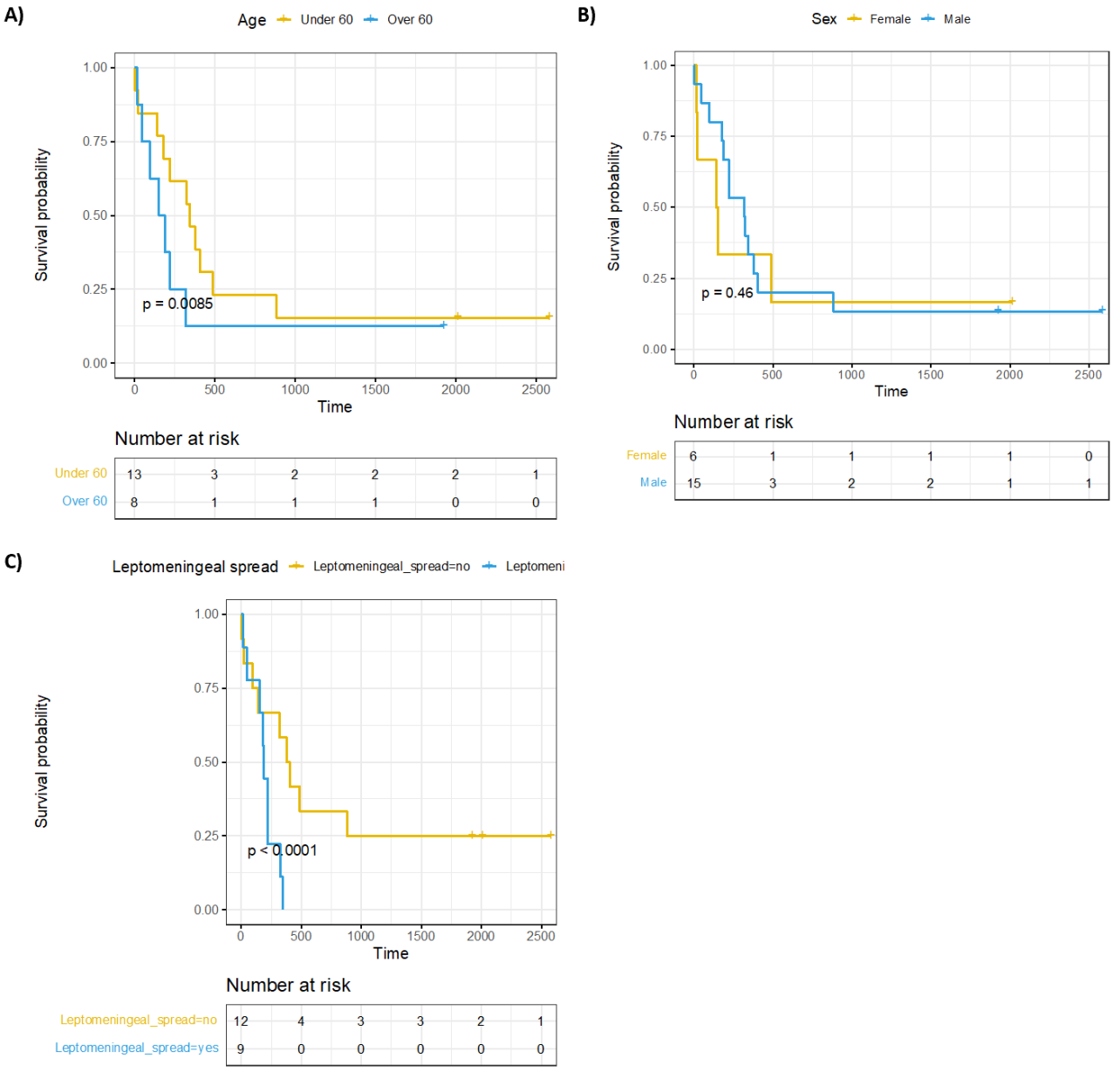

Figure 6. Survival analysis. Kaplan-Meier survival curves comparing A) patients age groups, B) patients' sex, C) leptomeningeal spread status.

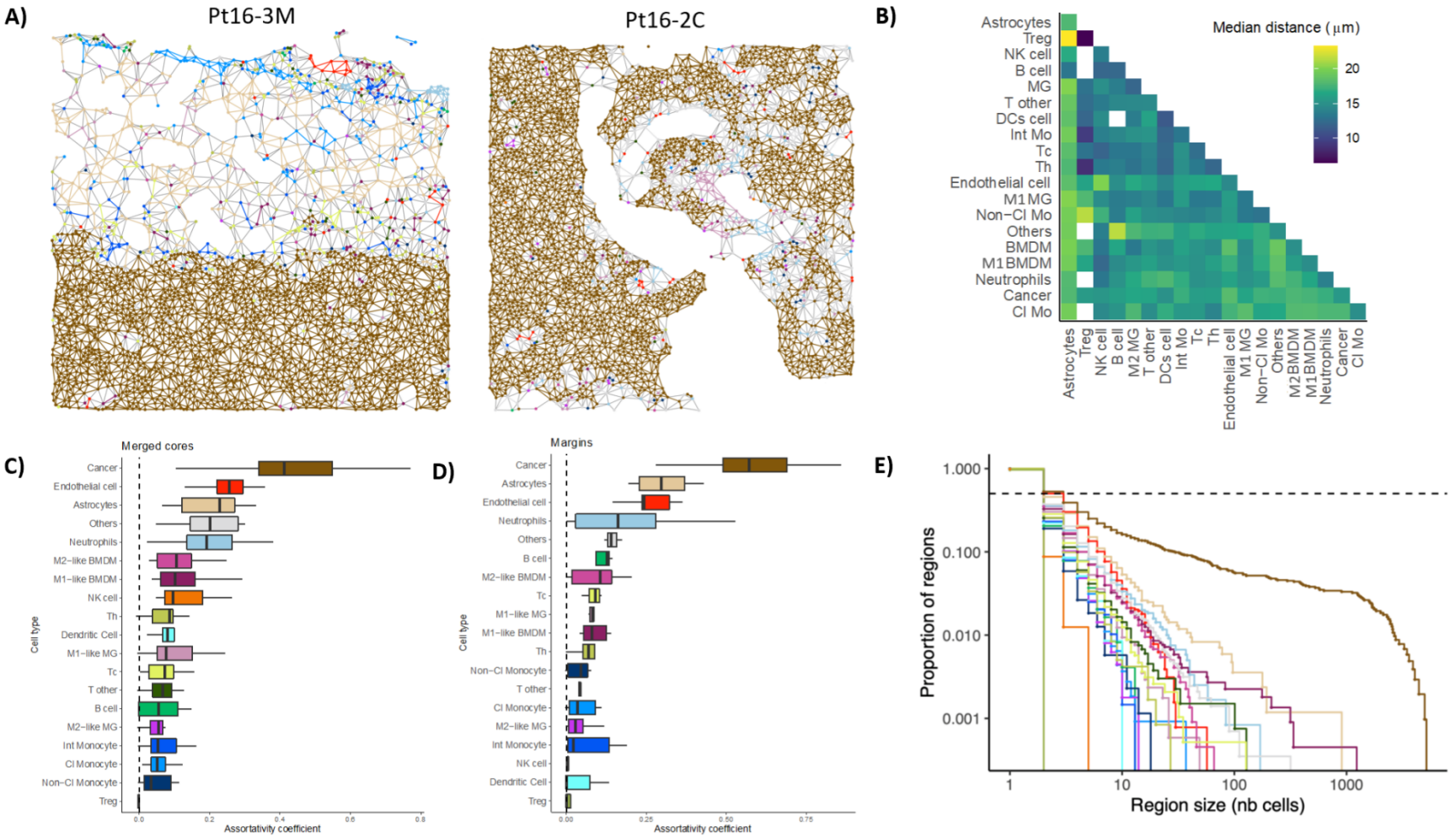

Figure 7. Spatial analysis. A) Spatial graphs of a margin sample (left) and a core sample (right) of patient 16. B) Heatmap representing the median distance (in micrometers) between pairs of neighboring cells. White squares mean those two cell types did not co-occur together. C) Assortativity of merged cores samples. D) Assortativity of margin samples. E) Proportion of regions found within the region of size.

Next, we looked at the difference in cell type proportion between groups. First, the cell type proportion was compared between core and margin samples. Core samples tend to have significantly more cancer cells (p= 0.0143), less astrocytes (p = 0.0015), less M1-like microglia (p=0.0110) and less T helper cells (p=0.0365) compared to margin samples (Figure 5A). When looking at only tumor samples that have both a margin and a core, there is no statistical difference in composition between their margin and core samples (Supplementary Figure S3A).

Secondly, we looked at leptomeningeal spread status. Core samples of patient that presented with leptomeningeal spread had more cancer cells (p= 0.0031), less immune infiltration of neutrophils (p= 0.0008), M1-like macrophages (p= 0.0310) and T other cell (p=0,0200) in their microenvironment (Figure 5B). When looking at only margin samples, there is no statistical differences between the two groups (Supplementary Figure S3B).

Thirdly, no statistical differences regarding the immune composition of the microenvironment have been found when comparing alive and deceased patients (Figure 5C).

4.1.5 Survival analysis

In the Kaplan-Meier survival analysis, it was observed that younger patients have a significantly higher survival rate compared to older patients (p=0.0085) (Figure 6A). Sex did not have a significant influence on survival (p=0.46) (Figure 6B). Also, patients without leptomeningeal spread had a better overall survival ($p < 0.0001$) (Figure 6C).

4.1.6 Spatial analysis

Next, spatial information was analyzed by examining the cell-cell interaction between the different cell types. A Delaunay triangulation was used to create spatial graphs for each tissue samples. Different patterns between margin and core samples were observed (Figure 7A). Most margin samples have a clear border separating the normal brain tissue cells (astrocytes) from the densely packed tumor cells. In contrast, in core samples we observe cancer cells throughout.

After, the distance between neighboring cells was analyzed (Figure 7B). The smallest distances were between T reg and Treg cells (5 um) and the largest distances were observed between astrocytes and T reg (25 um).

Then, the assortativity of cells was analyzed to examine the mixing between cells (Figure 7C and D). All cell types had a positive assortativity coefficient meaning cells tend to touch cells of the same type. In both core and margin samples, cancer cells were the most assortative cell type. The endothelial cells have a high assortativity score. Astrocytes were more assortative in margin samples.

Next, we examine regions where the connected cells are of the same type (Figure 7E). All cell types had a heavy-tailed distribution with 50% of cells belonging to a region size of one. Of the cell types that do have large regions, most of them are cancer cells. Cancer cells tend to cluster together in larger groups compared to any other cells type. 50 % of cells found within large regions belong to cancer cells (Supplementary Figure S4). The second highest proportion of cells belonging to large regions are astrocytes.

Finally, the median distance between cancer cells to all the cell types was analyzed. Margin samples tend to have a smaller median distance between cancer cells and other immune cell types such as M1-like MG, non-classical monocyte, T other and Tc (Figure 8A). However, the Z score does not show this difference (Supplementary Figure S5A). Patients without leptomeningeal spread, have smaller median distance between cancer cells and other immune cell types such as neutrophils, M1-like MG and Int Monocytes (Figure 8B). However, the Z score does not show this difference (Supplementary Figure S5B). Deceased patients had a smaller median distance between cancer cells and endothelial cells (Figure 8C). However, the Z score does not show this difference (Supplementary Figure S5C).

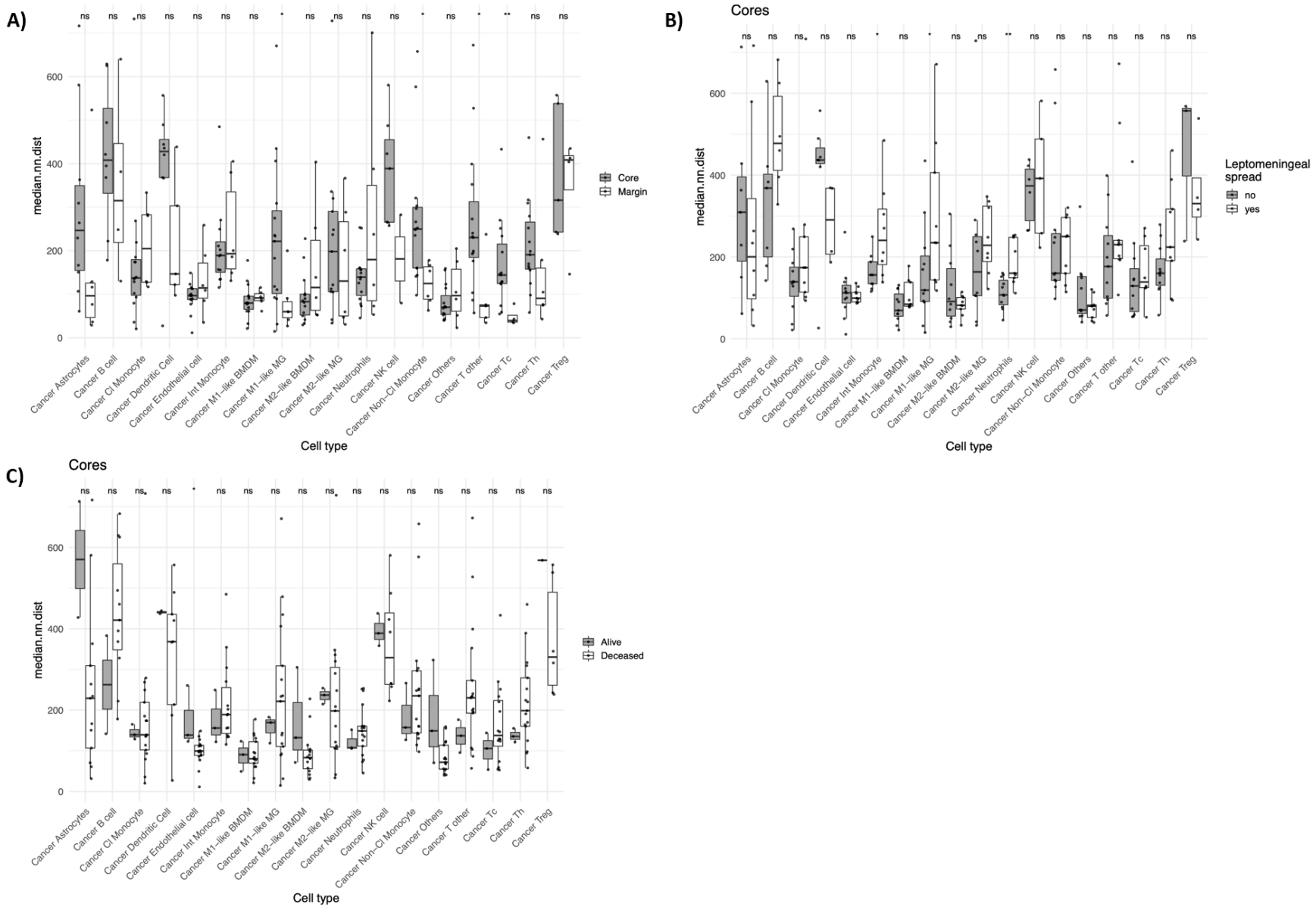

Figure 8. Comparison of median distance of cancer cells and the other cell types of A) Core and margin, B) Leptomeningeal status, C) alive and deceased.

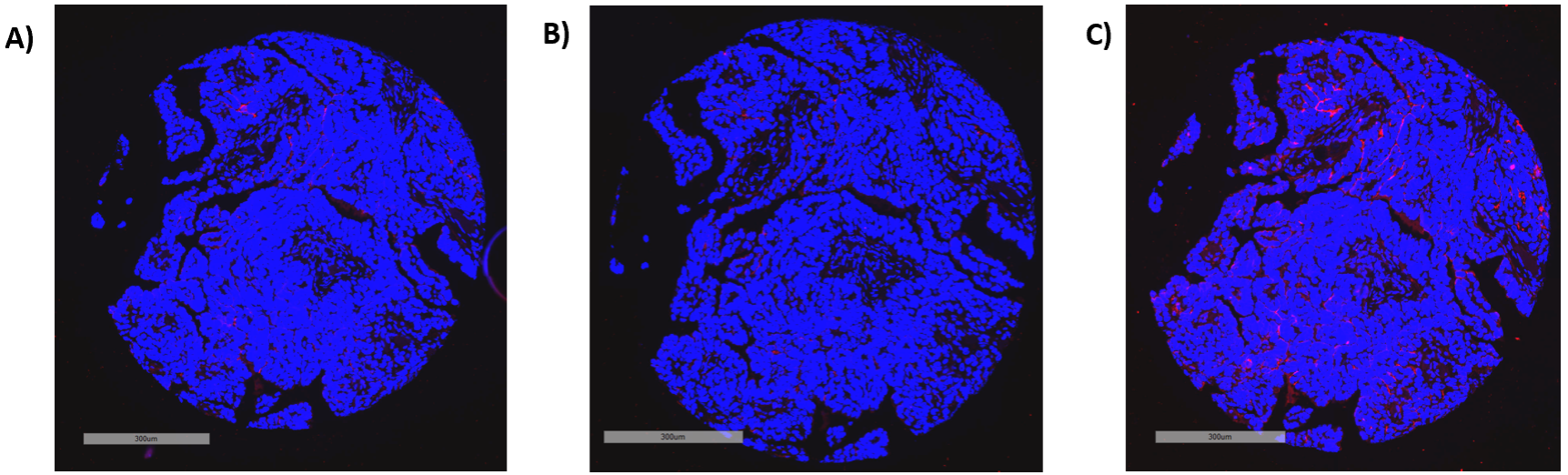

Figure 9. Immunofluorescence of CD73 staining patterns. Representative image of CD73 staining at different concentrations: Concentration at A) 1/800, B) 1/400, C) 1/200. The blue represents DAPI (nuclei) and the red represents CD73 binding.

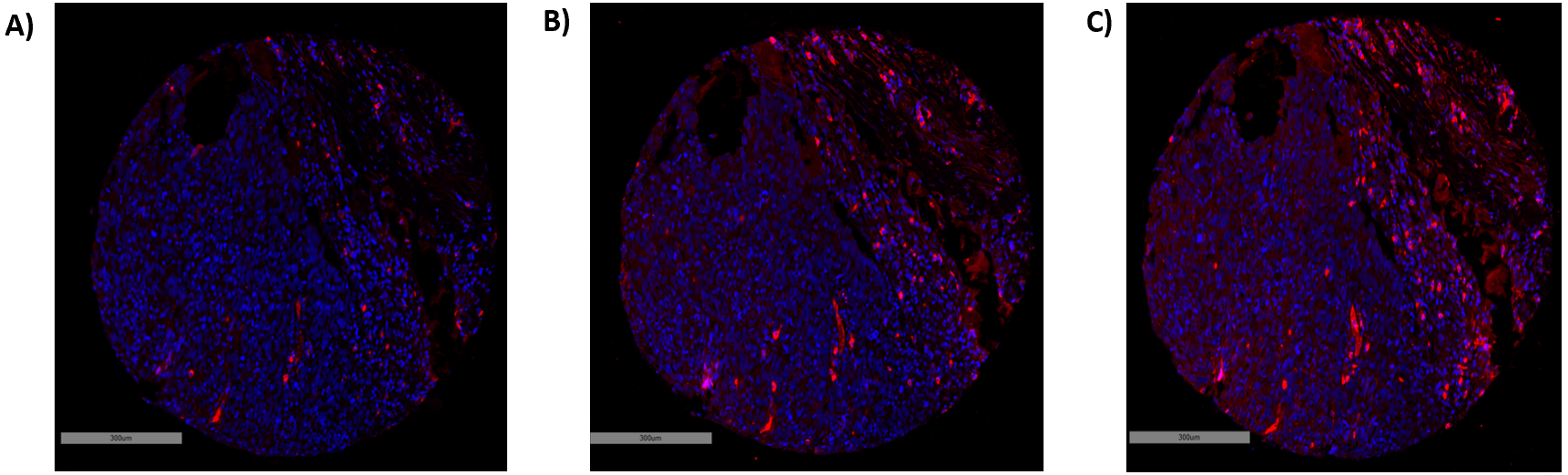

Figure 10. Immunofluorescence of A2a staining patterns. Representative images of A2a staining at different concentrations: Concentration at A) 1/200, B) 1/100, C) 1/50. The blue represents DAPI (nuclei) and the red represents A2a binding.

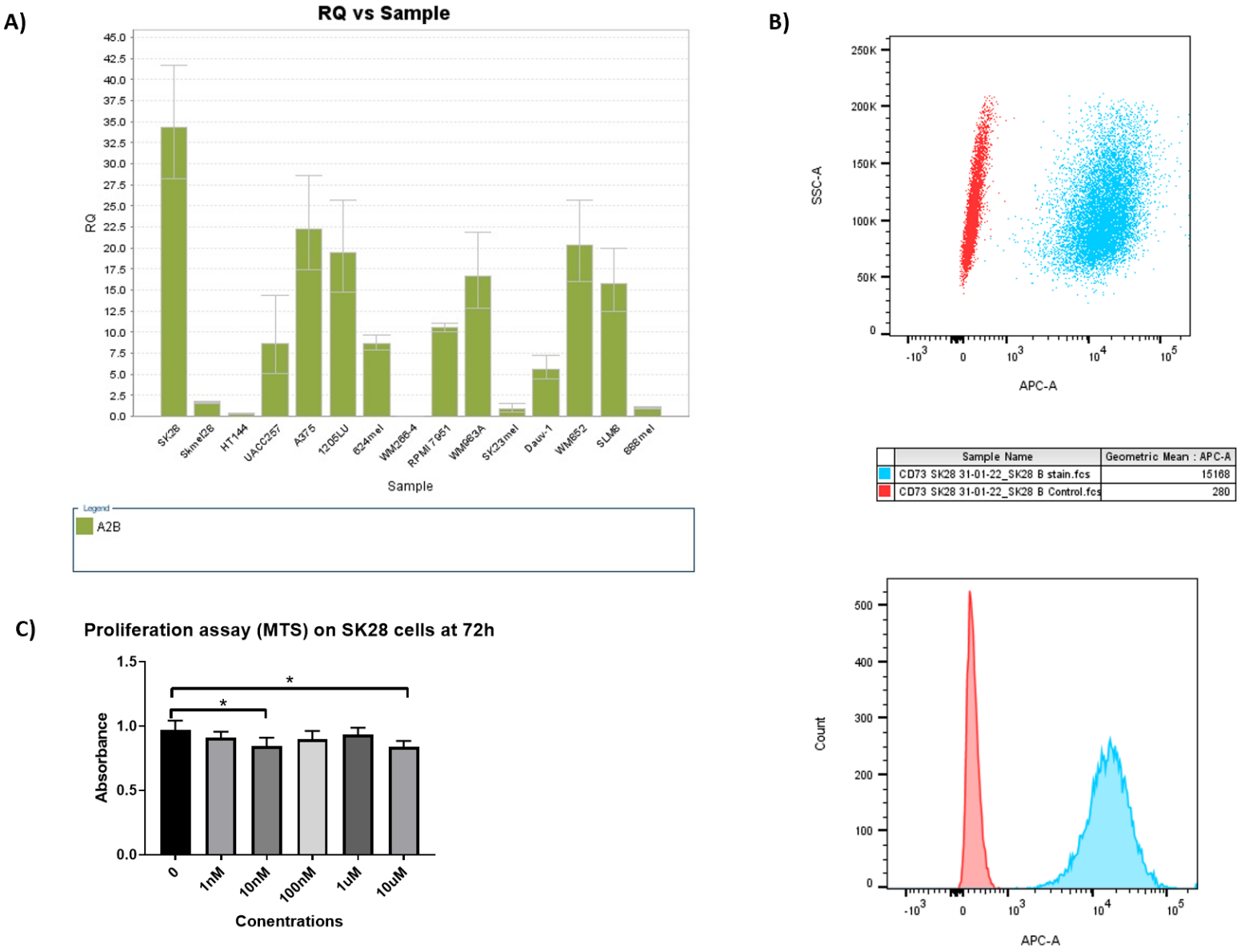

Figure 11. Proliferation of SK28 cell line. A) The expression of A2b receptor on melanoma cell lines using QPCR. RQ: Relative Quantification. B) Determining the expression of CD73 using FACS. C) Proliferation assay (MTS) at 72h when adding A2b agonist (BAY) at different concentrations.

4.1.7 Optimize antibodies of the adenosine pathway (CD73 and A2a) for CyTOF IMC

The optimization of CD73 antibody was successfully done. Less background noise was observed for concentration of 1/800 (Figure 9A) compared to concentration of 1/400 (Figure 9B) and 1/200 (Figure 9C). The optimization of A2a antibody was successfully done. Less background noise was observed for concentration of 1/200 (Figure 10A) compared to concentration of 1/100 (Figure 10B) and 1/50 (Figure 10C).

4.2 Aim 2

The expression level of A2b is heterogenous between the different cell types (Figure 11A). The cell line that expressed the most A2b level was SK28 cell line. SK28 cell line was also positive for CD73 antibody (Figure 11B). Next, the proliferation of SK28 cells was analyzed in different conditions. The MTS method was used to access the proliferation of SK28 cells. The proliferation of SK28 cells was first analyzed when adding an agonist of A2b receptor, BAY. There is a statistical difference between the control and BAY concentrated at 10 nM ($p= 0.0050$) and 10uM ($p= 0.0014$) (Figure 11C). The proliferation of SK28 cell was then analyzed when adding AMP to stimulate CD73 receptor. There is no statistical differences between the different conditions (Supplementary Figure S6A).

Next, when performing an IncuCyte, to access the proliferation of SK28 cells, there was no statistical difference in proliferation when adding BAY, an agonist of A2b receptor, to the SK28 cell line ($p= 0.7320$) (Supplementary Figure S6B). Also, there was no statistical difference in proliferation when adding PSB, an antagonist for A2b receptor, to the SK28 cell line ($p=0,8491$) (Supplementary Figure S6B).

5. Chapter 5 – Discussion

5.1 Aim 1

We were able to spatially map the immune landscape of melanoma using imaging mass cytometry and in total, we were able to classify 142 875 cells total, 126 602 cells from core samples and 16 273 cells from margin samples, from 48 samples. Heterogeneity was observed between the different melanoma samples, and this is consistent with the current literature (58, 115). In a study by Samalley et al. (2021), they found that melanoma metastases of the brain contain more melanoma cells, low NK cells and some B cells whereas metastases of the skin contain more fibroblasts and highest number of B cells (115). It was observed across all our melanoma samples that macrophages are amongst the most common immune cells (Figure 4A), which is in accordance with the current literature. A study by Moldoveanu et al. (2022) supports our finding with their most common immune infiltrate being monocytes/macrophages (58). In a study by Karimi et al. (2023), they also found that macrophages were an abundant cell type amongst all cells in the TME (60). A study by Emri et al. (2012), observed that a high number of macrophages within the melanoma microenvironment was associated with a poor prognosis (116) but no significant difference was found in our analysis (Figure 5C). Cancer cells tended to cluster together in larger groups compared to any other cell type (Figure 3D), and this pattern is consisting with what Moldoveanu et al. (2022) found in their study (58).

In our dataset, T cell infiltration was minimal in our melanoma brain metastasis samples (Figure 4D) and this finding is concurrent with the literature (5, 117). In a study by Weiss et al. (2021) on paired intracerebral and extracerebral melanoma metastases, it was found that T cell (CD3+, CD8+) infiltration is lower in melanoma brain metastases compared to extracranial sites (118). This lower T cell infiltration in melanoma brain metastasis compared to extracranial sites has also been found in a study by Herrera-Rios et al. (2020) (119). The complex mechanism underlining the reduction level of T cells is not completely understood. However, studies have shown that microglia could be implicated by limiting T cell infiltration (120, 121).

In our dataset, there are three patients that are alive and responded to immunotherapy treatment. No statistical differences regarding the immune composition of the microenvironment have been found when comparing alive and deceased patients (Figure 5C). However, a trend was observed. Patients that are alive tend to have more T cell infiltration in their microenvironment compared to patients that are deceased. In concordance with the literature, having tumor-infiltrating lymphocytes cells in the microenvironment of tumors has been shown to be associated with a better prognostic to ICI therapy and poorly infiltrated tumors with immune cells respond worse to immunotherapy (58, 122, 123). In a study by Azimi et al. (2012), the researchers analyzed whether the density and distribution of tumor-infiltrating lymphocytes could influence primary cutaneous melanoma progression to lymph nodes and looked at overall survival for 1,138 patients (122). They found a directly proportional correlation between the amount of tumor infiltrating lymphocytes and lymph node involvement and overall survival. The exact mechanism of T cell migration to the tumor site is unknown but it was proposed that putative targets for lymphocytes such as tumor specific antigens, tissue specific antigens and common cancer specific antigens can attract lymphocytes. It is unclear however if the lymphocyte infiltration is mediated by the normal immune response, the tumor or it's microenvironment. Also, in a study by Hamid et al. (2011), they found that an increased infiltration of T cells is associated with an increased pharmacological effectiveness of ipilimumab (123).

It was observed that there is an increased presence of astrocytes in tumor margins compared to tumor cores (Figure 5A). This may be explained by the fact that astrocytes are part of the normal brain tissue and that tumors disturb the physiological distribution of cells within tissues. Additionally, when only analyzing a sub-set of patients that have both a tumor core and tumor margin sample, we did not find a significant difference. This could be explained by a small patient sample (n=5, Supplementary Figure S3A) which led to poorer statistical analysis strength. However, the same trend as tumor margins compared to tumor cores (Figure 5A) was observed. It was also observed that the overall survival of patients with leptomeningeal spread was worse compared to patients without leptomeningeal spread, which is consistent with the current literature (41, 44, 124). Patients with leptomeningeal spread have significantly less neutrophils,

M1-like BMDM, T other cells and more cancer cells with a bigger median distance between cancer cells and neutrophils (Figure 5B, 8B). Hence, leptomeningeal spread seems to be associated with less immune infiltration in the microenvironment. This finding has also been observed in a study by Smalley et al. (2021) characterizing the immune microenvironment of 43 samples including skin metastases, melanoma brain metastasis and melanoma leptomeningeal spread. They discovered that melanoma leptomeningeal metastasis was associated with an immune-suppressed T-cell microenvironment compared to skin and brain metastases (115). In our spatial analysis, we found that all cell types followed a heavy-tailed distribution with 50% of cells belong to a region size of one. This finding was also observed in Moldoveanu et al. (2022) analysis.

5.2 Aim 2

According to the literature, when adding the A2b adenosine receptor selective agonist BAY, to melanoma cells it causes an increase in cell proliferation (107). In our study, we found that adding BAY, concentrated at 10 uM to melanoma SK28 line cells (Figure 11C), caused a decrease in cell proliferation which rebuts our hypothesis.

The proliferative and antiproliferative effects of adenosine receptors are regulated by complex mechanisms and mediated by a variety of second messengers. It has been shown that A2b can regulate increase of cAMP levels (78). cAMP is involved in tumor suppressive pathways in different types of cancer (125). In our study, the antiproliferative effect that we found when adding BAY to SK28 cells could be explained by the increase in cAMP which can activate downstream signaling pathways such as cAMP/PKA, cAMP/CREB, Ras-MAPK, and EPAC/Rap1 (125).

Another explanation could be the fact that A2b has been linked with the p53 gene which is known for its function in cell growth arrest, DNA repair and apoptosis (126). In a study by Long et al. (2013), they demonstrated that activation of the A2b receptor significantly increased cell death mediated via p53 upon accumulation of extracellular adenosine (126). In their study, they knocked down A2b receptors and stimulated cells with adenosine and p53 agonist and they

found that expression of A2b receptor was down by 80% while p53 expression was unchanged. In addition, they found that using an A2b receptor antagonist and p53 agonist reduced cell death by approximately 50%. This suggests that p53 induces A2b receptor expression and that A2b has a significant role in cell death downstream of p53 in the presence of adenosine.

Another mechanism that could explain A2b's anti-proliferative role is that it activates the mitochondrial caspase-9 apoptotic pathway. In the study by Long et al. (2013), they transiently expressed A2b receptor in Saos-2 cells and assessed the cell-cycle distribution after 48h and they found that some cells were in the sub-G1 phase which is an indication of cell death (126). Then, they added an adenosine analog and found cell death levels further increased. Interestingly, they found that pre-treatment of cells with a pan-caspase inhibitor zVADfmk completely prevented cell death suggesting that the mechanism of A2b induced cell death is caspase-dependent (126). To find through which caspases A2b acted, they used cell extracts and western blots to find that upon agonist stimulation of A2b, there are increased levels of caspase 9 suggesting cell death mediation through the mitochondrial caspase-9 apoptotic pathway (126). Hence, the results we found in our analysis, could be explained by these mechanisms above. However, more research needs to be done to confirm this finding.

There is a statistical difference between the control and BAY concentrated at 10 nM. This finding is an abnormal result regarding the 10 nM. The exact threshold activation for the A2b receptor is unknow and depends on a variety of experimental factors. Currently there seems to be a lack of theoretical explanation that could account for this outlier result. For the 10 nM concentrations the significance difference could be attributed to a manipulation error.

6. Chapter 6 – Conclusion

We were able to spatially map the immune landscape of melanoma using IMC**.** With this panel, we were able to characterize the brain microenvironment of 21 melanoma brain metastasis patient and we were able to classify tumor cells, astrocytes, blood vessels, myeloid cells, and lymphoid cells. We observed that heterogeneity between samples with the most common immune infiltrate being macrophages and low T cell infiltration. In the microenvironment of patients with leptomeningeal spread, we observed more cancer cell and less neutrophils, M1-like BMDM, T other cells with a larger median distance between cancer cells and neutrophils. This study highlights the potential of multiplexed single cell technology to quantify spatial cell-cell interactions of melanoma brain metastasis. We were also able to successfully optimize antibodies of the adenosine pathway (CD73 and A2a) for a future CyTOF IMC panel. Also, we found that A2b receptor has an antiproliferative effect on melanoma cancer cells, but more research needs to be done to confirm this finding. In vivo analysis needs to be done using A2b receptor knocked-down mice in order to illustrate this finding.

References

1. Xiao Y, Yu D. Tumor microenvironment as a therapeutic target in cancer. Pharmacol Ther. 2021;221:107753.

2. Wang M, Zhao J, Zhang L, Wei F, Lian Y, Wu Y, et al. Role of tumor microenvironment in tumorigenesis. J Cancer. 2017;8(5):761-73.

3. Gentles AJ, Newman AM, Liu CL, Bratman SV, Feng W, Kim D, et al. The prognostic landscape of genes and infiltrating immune cells across human cancers. Nat Med. 2015;21(8):938-45.

4. Cassetta L, Pollard JW. Tumor-associated macrophages. Curr Biol. 2020;30(6):R246-r8.

5. Westphal D, Glitza Oliva IC, Niessner H. Molecular insights into melanoma brain metastases. Cancer. 2017;123(S11):2163-75.

6. Chee DO, Townsend CM, Jr., Galbraith MA, Eilber FR, Morton DL. Selective reduction of human tumor cell populations by human granulocytes in vitro. Cancer Res. 1978;38(12):4534-9.

7. Gerrard TL, Cohen DJ, Kaplan AM. Human neutrophil-mediated cytotoxicity to tumor cells. J Natl Cancer Inst. 1981;66(3):483-8.

8. Granot Z, Henke E, Comen EA, King TA, Norton L, Benezra R. Tumor entrained neutrophils inhibit seeding in the premetastatic lung. Cancer Cell. 2011;20(3):300-14.

9. Cameron DJ. A comparison of the cytotoxic potential in polymorphonuclear leukocytes obtained from normal donors and cancer patients. Clin Immunol Immunopathol. 1983;28(1):115-24.

10. Coffelt SB, Wellenstein MD, de Visser KE. Neutrophils in cancer: neutral no more. Nat Rev Cancer. 2016;16(7):431-46.

11. Galdiero MR, Varricchi G, Loffredo S, Mantovani A, Marone G. Roles of neutrophils in cancer growth and progression. J Leukoc Biol. 2018;103(3):457-64.

12. Shaul ME, Fridlender ZG. Neutrophils as active regulators of the immune system in the tumor microenvironment. J Leukoc Biol. 2017;102(2):343-9.

13. Sionov RV, Fridlender ZG, Granot Z. The Multifaceted Roles Neutrophils Play in the Tumor Microenvironment. Cancer Microenviron. 2015;8(3):125-58.

14. Granot Z, Fridlender ZG. Plasticity beyond cancer cells and the "immunosuppressive switch". Cancer Res. 2015;75(21):4441-5.

15. Guthrie GJ, Charles KA, Roxburgh CS, Horgan PG, McMillan DC, Clarke SJ. The systemic inflammation-based neutrophil-lymphocyte ratio: experience in patients with cancer. Crit Rev Oncol Hematol. 2013;88(1):218-30.

16. Gungabeesoon J, Gort-Freitas NA, Kiss M, Bolli E, Messemaker M, Siwicki M, et al. A neutrophil response linked to tumor control in immunotherapy. Cell. 2023;186(7):1448-64.e20.

17. Ager A. Cancer immunotherapy: T cells and neutrophils working together to attack cancers. Cell. 2023;186(7):1304-6.

18. Quail DF, Joyce JA. The Microenvironmental Landscape of Brain Tumors. Cancer Cell. 2017;31(3):326-41.

19. Brandao M, Simon T, Critchley G, Giamas G. Astrocytes, the rising stars of the glioblastoma microenvironment. Glia. 2019;67(5):779-90.

20. Marchetti D, Li J, Shen R. Astrocytes contribute to the brain-metastatic specificity of melanoma cells by producing heparanase. Cancer Res. 2000;60(17):4767-70.

21. Klein A, Schwartz H, Sagi-Assif O, Meshel T, Izraely S, Ben Menachem S, et al. Astrocytes facilitate melanoma brain metastasis via secretion of IL-23. J Pathol. 2015;236(1):116-27.

22. Nicolson GL, Menter DG. Trophic factors and central nervous system metastasis. Cancer Metastasis Rev. 1995;14(4):303-21.

23. Preston AN, Cervasio DA, Laughlin ST. Visualizing the brain's astrocytes. Methods Enzymol. 2019;622:129-51.

24. Nolte C, Matyash M, Pivneva T, Schipke CG, Ohlemeyer C, Hanisch UK, et al. GFAP promoter-controlled EGFP-expressing transgenic mice: a tool to visualize astrocytes and astrogliosis in living brain tissue. Glia. 2001;33(1):72-86.

25. Melanoma Skin Cancer: Gouverment of Canada; 2019 [cited 2022 November 8]. Available from: https://www.canada.ca/en/public-health/services/chronic-diseases/cancer/melanoma-skin-cancer.html?fbclid=IwAR3CRw8zDZKz3_v2RDv5rLA-KoVx-gGhZqst-Kxp5xCXTt5Qe_0XmdelJz4

26. Cancer Facts & Figures American Cancer Society2022 [cited 2022 November 8]. Available from: https://www.cancer.org/content/dam/cancer-org/research/cancer-facts-and-statistics/annual-cancer-facts-and-figures/2022/2022-cancer-facts-and-figures.pdf.

27. Key Statistics for Melanoma Skin Cancer American Cancer Society [updated 2023; cited 2022 November 8]. Available from: https://www.cancer.org/cancer/melanoma-skin-cancer/about/key-statistics.html.

28. Non Melanoma Skin Cancer Government of Canada [updated 2019-12-09; cited 2022 November 8]. Available from: https://www.canada.ca/en/public-health/services/chronic-diseases/cancer/non-melanoma-skin-cancer.html?fbclid=IwAR0R3jukFEPAmzJv78txdLvgM0llSSpCcdeovEEWGz8P2stnLKS5h9MHRo4.

29. Key Statistics for Basal and Squamous Cell Skin Cancers American Cancer Society [cited 2022 November 8]. Available from: https://www.cancer.org/cancer/basal-and-squamous-cell-skin-cancer/about/key-statistics.html.

30. Survival statistics for non-melanoma skin cancer Canadian Cancer Society [cited 2022 November 8]. Available from: https://cancer.ca/en/cancer-information/cancer-types/skin-non-melanoma/prognosis-and-survival/survival-statistics

31. Li HO, Bailey AJ, Grose E, McDonald JT, Quimby A, Johnson-Obaseki S, et al. Socioeconomic Status and Melanoma in Canada: A Systematic Review. J Cutan Med Surg. 2021;25(1):87-94.

32. Canadian Cancer Statistics. Canadian Cancer Society; 2021.

33. Skin Cancer: Melanoma National Cancer institute [cited 2022 November 8]. Available from: https://training.seer.cancer.gov/melanoma/intro/.

34. Oba J, Woodman SE. The genetic and epigenetic basis of distinct melanoma types. J Dermatol. 2021;48(7):925-39.

35. Elder DE, Bastian BC, Cree IA, Massi D, Scolyer RA. The 2018 World Health Organization Classification of Cutaneous, Mucosal, and Uveal Melanoma: Detailed Analysis of 9 Distinct Subtypes Defined by Their Evolutionary Pathway. Arch Pathol Lab Med. 2020;144(4):500-22.

36. Damsky WE, Theodosakis N, Bosenberg M. Melanoma metastasis: new concepts and evolving paradigms. Oncogene. 2014;33(19):2413-22.

37. Sawaya R, Bindal RK, Lang FF, Suki D. Metastatic brain tumors. Brain tumors: Elsevier Ltd; 2012. p. 864-92.

38. Cohen JV, Tawbi H, Margolin KA, Amravadi R, Bosenberg M, Brastianos PK, et al. Melanoma central nervous system metastases: current approaches, challenges, and opportunities. Pigment Cell Melanoma Res. 2016;29(6):627-42.

39. Glitza Oliva I, Tawbi H, Davies MA. Melanoma Brain Metastases: Current Areas of Investigation and Future Directions. Cancer J. 2017;23(1):68-74.

40. Sacks P, Rahman M. Epidemiology of Brain Metastases. Neurosurg Clin N Am. 2020;31(4):481-8.

41. Nayar G, Ejikeme T, Chongsathidkiet P, Elsamadicy AA, Blackwell KL, Clarke JM, et al. Leptomeningeal disease: current diagnostic and therapeutic strategies. Oncotarget. 2017;8(42):73312-28.

42. Le Rhun E, Taillibert S, Chamberlain MC. Carcinomatous meningitis: Leptomeningeal metastases in solid tumors. Surg Neurol Int. 2013;4(Suppl 4):S265-88.

43. Leal T, Chang JE, Mehta M, Robins HI. Leptomeningeal Metastasis: Challenges in Diagnosis and Treatment. Curr Cancer Ther Rev. 2011;7(4):319-27.

44. Ferguson SD, Bindal S, Bassett RL, Jr., Haydu LE, McCutcheon IE, Heimberger AB, et al. Predictors of survival in metastatic melanoma patients with leptomeningeal disease (LMD). J Neurooncol. 2019;142(3):499-509.

45. Cheng H, Perez-Soler R. Leptomeningeal metastases in non-small-cell lung cancer. Lancet Oncol. 2018;19(1):e43-e55.

46. Smalley KS, Fedorenko IV, Kenchappa RS, Sahebjam S, Forsyth PA. Managing leptomeningeal melanoma metastases in the era of immune and targeted therapy. Int J Cancer. 2016;139(6):1195-201.

47. Figura NB, Rizk VT, Armaghani AJ, Arrington JA, Etame AB, Han HS, et al. Breast leptomeningeal disease: a review of current practices and updates on management. Breast Cancer Res Treat. 2019;177(2):277-94.

48. Le Rhun E, Guckenberger M, Smits M, Dummer R, Bachelot T, Sahm F, et al. EANO-ESMO Clinical Practice Guidelines for diagnosis, treatment and follow-up of patients with brain metastasis from solid tumours. Ann Oncol. 2021;32(11):1332-47.

49. Pasquali S, Hadjinicolaou AV, Chiarion Sileni V, Rossi CR, Mocellin S. Systemic treatments for metastatic cutaneous melanoma. Cochrane Database Syst Rev. 2018;2(2):Cd011123.

50. Tawbi H. The standard of care for brain metastases in melanoma. Clin Adv Hematol Oncol. 2020;18(1):28-31.

51. Hong AM, Fogarty GB, Dolven-Jacobsen K, Burmeister BH, Lo SN, Haydu LE, et al. Adjuvant Whole-Brain Radiation Therapy Compared With Observation After Local Treatment of Melanoma Brain Metastases: A Multicenter, Randomized Phase III Trial. J Clin Oncol. 2019;37(33):3132-41.

52. Ralli M, Botticelli A, Visconti IC, Angeletti D, Fiore M, Marchetti P, et al. Immunotherapy in the Treatment of Metastatic Melanoma: Current Knowledge and Future Directions. J Immunol Res. 2020;2020:9235638.

53. Carlino MS, Larkin J, Long GV. Immune checkpoint inhibitors in melanoma. Lancet. 2021;398(10304):1002-14.

54. Wei SC, Duffy CR, Allison JP. Fundamental Mechanisms of Immune Checkpoint Blockade Therapy. Cancer Discov. 2018;8(9):1069-86.

55. Sun J, Kroeger JL, Markowitz J. Introduction to Multiparametric Flow Cytometry and Analysis of High-Dimensional Data. Methods Mol Biol. 2021;2194:239-53.

56. Veenstra J, Dimitrion P, Yao Y, Zhou L, Ozog D, Mi QS. Research Techniques Made Simple: Use of Imaging Mass Cytometry for Dermatological Research and Clinical Applications. J Invest Dermatol. 2021;141(4):705-12.e1.

57. Martinez-Morilla S, Villarroel-Espindola F, Wong PF, Toki MI, Aung TN, Pelekanou V, et al. Biomarker Discovery in Patients with Immunotherapy-Treated Melanoma with Imaging Mass Cytometry. Clin Cancer Res. 2021;27(7):1987-96.

58. Moldoveanu D, Ramsay L, Lajoie M, Anderson-Trocme L, Lingrand M, Berry D, et al. Spatially mapping the immune landscape of melanoma using imaging mass cytometry. Sci Immunol. 2022;7(70):eabi5072.

59. Tantalo D, Nguyen T, Yeang HXA, Zhu J, Macdonald S, Wang M, et al. Using Mass Cytometry to Analyze the Tumor-Infiltrating Lymphocytes in Human Melanoma. Methods Mol Biol. 2021;2265:543-55.

60. Karimi E, Yu MW, Maritan SM, Perus LJM, Rezanejad M, Sorin M, et al. Single-cell spatial immune landscapes of primary and metastatic brain tumours. Nature. 2023;614(7948):555-63.

61. Borea PA, Gessi S, Merighi S, Varani K. Adenosine as a Multi-Signalling Guardian Angel in Human Diseases: When, Where and How Does it Exert its Protective Effects? Trends Pharmacol Sci. 2016;37(6):419-34.

62. Bahreyni A, Khazaei M, Rajabian M, Ryzhikov M, Avan A, Hassanian SM. Therapeutic potency of pharmacological adenosine receptor agonist/antagonist in angiogenesis, current status and perspectives. J Pharm Pharmacol. 2018;70(2):191-6.

63. Fredholm BB, AP IJ, Jacobson KA, Klotz KN, Linden J. International Union of Pharmacology. XXV. Nomenclature and classification of adenosine receptors. Pharmacol Rev. 2001;53(4):527-52.

64. Zimmermann H. Extracellular metabolism of ATP and other nucleotides. Naunyn Schmiedebergs Arch Pharmacol. 2000;362(4-5):299-309.

65. Yegutkin GG. Nucleotide- and nucleoside-converting ectoenzymes: Important modulators of purinergic signalling cascade. Biochim Biophys Acta. 2008;1783(5):673-94.

66. Allard B, Allard D, Buisseret L, Stagg J. The adenosine pathway in immuno-oncology. Nat Rev Clin Oncol. 2020;17(10):611-29.

67. Haskó G, Cronstein BN. Adenosine: an endogenous regulator of innate immunity. Trends Immunol. 2004;25(1):33-9.

68. Vijayan D, Young A, Teng MWL, Smyth MJ. Targeting immunosuppressive adenosine in cancer. Nat Rev Cancer. 2017;17(12):709-24.

69. van Calker D, Müller M, Hamprecht B. Adenosine regulates via two different types of receptors, the accumulation of cyclic AMP in cultured brain cells. J Neurochem. 1979;33(5):999-1005.

70. Ralevic V, Burnstock G. Receptors for purines and pyrimidines. Pharmacol Rev. 1998;50(3):413-92.

71. Ohta A, Sitkovsky M. Role of G-protein-coupled adenosine receptors in downregulation of inflammation and protection from tissue damage. Nature. 2001;414(6866):916-20.

72. Borea PA, Gessi S, Merighi S, Vincenzi F, Varani K. Pathological overproduction: the bad side of adenosine. Br J Pharmacol. 2017;174(13):1945-60.

73. Mirza A, Basso A, Black S, Malkowski M, Kwee L, Pachter JA, et al. RNA interference targeting of A1 receptor-overexpressing breast carcinoma cells leads to diminished rates of cell proliferation and induction of apoptosis. Cancer Biol Ther. 2005;4(12):1355-60.

74. Dastjerdi MN, Rarani MZ, Valiani A, Mahmoudieh M. The effect of adenosine A1 receptor agonist and antagonist on p53 and caspase 3, 8, and 9 expression and apoptosis rate in MCF-7 breast cancer cell line. Res Pharm Sci. 2016;11(4):303-10.

75. Palmer TM, Trevethick MA. Suppression of inflammatory and immune responses by the A(2A) adenosine receptor: an introduction. Br J Pharmacol. 2008;153 Suppl 1(Suppl 1):S27-34.

76. Ohta A, Gorelik E, Prasad SJ, Ronchese F, Lukashev D, Wong MK, et al. A2A adenosine receptor protects tumors from antitumor T cells. Proc Natl Acad Sci U S A. 2006;103(35):13132-7.

77. Merighi S, Mirandola P, Milani D, Varani K, Gessi S, Klotz KN, et al. Adenosine receptors as mediators of both cell proliferation and cell death of cultured human melanoma cells. J Invest Dermatol. 2002;119(4):923-33.

78. Sun Y, Huang P. Adenosine A2B Receptor: From Cell Biology to Human Diseases. Front Chem. 2016;4:37.

79. Stagg J, Divisekera U, McLaughlin N, Sharkey J, Pommey S, Denoyer D, et al. Anti-CD73 antibody therapy inhibits breast tumor growth and metastasis. Proc Natl Acad Sci U S A. 2010;107(4):1547-52.

80. Mittal D, Sinha D, Barkauskas D, Young A, Kalimutho M, Stannard K, et al. Adenosine 2B Receptor Expression on Cancer Cells Promotes Metastasis. Cancer Res. 2016;76(15):4372-82.

81. Kasama H, Sakamoto Y, Kasamatsu A, Okamoto A, Koyama T, Minakawa Y, et al. Adenosine A2b receptor promotes progression of human oral cancer. BMC Cancer. 2015;15:563.

82. Ma DF, Kondo T, Nakazawa T, Niu DF, Mochizuki K, Kawasaki T, et al. Hypoxia-inducible adenosine A2B receptor modulates proliferation of colon carcinoma cells. Hum Pathol. 2010;41(11):1550-7.

83. Wei Q, Costanzi S, Balasubramanian R, Gao ZG, Jacobson KA. A2B adenosine receptor blockade inhibits growth of prostate cancer cells. Purinergic Signal. 2013;9(2):271-80.

84. Vecchio EA, Tan CY, Gregory KJ, Christopoulos A, White PJ, May LT. Ligand-Independent Adenosine A2B Receptor Constitutive Activity as a Promoter of Prostate Cancer Cell Proliferation. J Pharmacol Exp Ther. 2016;357(1):36-44.

85. Cekic C, Sag D, Li Y, Theodorescu D, Strieter RM, Linden J. Adenosine A2B receptor blockade slows growth of bladder and breast tumors. J Immunol. 2012;188(1):198-205.

86. Sun Y, Duan Y, Eisenstein AS, Hu W, Quintana A, Lam WK, et al. A novel mechanism of control of NFκB activation and inflammation involving A2B adenosine receptors. J Cell Sci. 2012;125(Pt 19):4507-17.

87. Itakura E, Huang RR, Wen DR, Paul E, Wünsch PH, Cochran AJ. IL-10 expression by primary tumor cells correlates with melanoma progression from radial to vertical growth phase and development of metastatic competence. Mod Pathol. 2011;24(6):801-9.

88. Yue FY, Geertsen R, Hemmi S, Burg G, Pavlovic J, Laine E, et al. IL-12 directly up-regulates the expression of HLA class I, HLA class II and ICAM-1 on human melanoma cells: a mechanism for its antitumor activity? Eur J Immunol. 1999;29(6):1762-73.

89. Donia M, Kjeldsen JW, Svane IM. The controversial role of TNF in melanoma. Oncoimmunology. 2016;5(4):e1107699.

90. Pacheco R, Martinez-Navio JM, Lejeune M, Climent N, Oliva H, Gatell JM, et al. CD26, adenosine deaminase, and adenosine receptors mediate costimulatory signals in the immunological synapse. Proc Natl Acad Sci U S A. 2005;102(27):9583-8.

91. Jafari SM, Panjehpour M, Aghaei M, Joshaghani HR, Enderami SE. A3 Adenosine Receptor Agonist Inhibited Survival of Breast Cancer Stem Cells via GLI-1 and ERK1/2 Pathway. J Cell Biochem. 2017;118(9):2909-20.

92. Nagaya H, Gotoh A, Kanno T, Nishizaki T. A3 adenosine receptor mediates apoptosis in in vitro RCC4-VHL human renal cancer cells by up-regulating AMID expression. J Urol. 2013;189(1):321-8.

93. Tsuchiya A, Nishizaki T. Anticancer effect of adenosine on gastric cancer via diverse signaling pathways. World J Gastroenterol. 2015;21(39):10931-5.

94. Kanno T, Gotoh A, Fujita Y, Nakano T, Nishizaki T. A(3) adenosine receptor mediates apoptosis in 5637 human bladder cancer cells by G(q) protein/PKC-dependent AIF upregulation. Cell Physiol Biochem. 2012;30(5):1159-68.

95. Vaupel P, Mayer A. Hypoxia-Driven Adenosine Accumulation: A Crucial Microenvironmental Factor Promoting Tumor Progression. Adv Exp Med Biol. 2016;876:177-83.

96. Kazemi MH, Raoofi Mohseni S, Hojjat-Farsangi M, Anvari E, Ghalamfarsa G, Mohammadi H, et al. Adenosine and adenosine receptors in the immunopathogenesis and treatment of cancer. J Cell Physiol. 2018;233(3):2032-57.

97. Montinaro A, Iannone R, Pinto A, Morello S. Adenosine receptors as potential targets in melanoma. Pharmacol Res. 2013;76:34-40.

98. Stagg J, Smyth MJ. Extracellular adenosine triphosphate and adenosine in cancer. Oncogene. 2010;29(39):5346-58.

99. Sorrentino R, Pinto A, Morello S. The adenosinergic system in cancer: Key therapeutic target. Oncoimmunology. 2013;2(1):e22448.

100. Young A, Ngiow SF, Madore J, Reinhardt J, Landsberg J, Chitsazan A, et al. Targeting Adenosine in BRAF-Mutant Melanoma Reduces Tumor Growth and Metastasis. Cancer Res. 2017;77(17):4684-96.

101. Loi S, Pommey S, Haibe-Kains B, Beavis PA, Darcy PK, Smyth MJ, et al. CD73 promotes anthracycline resistance and poor prognosis in triple negative breast cancer. Proc Natl Acad Sci U S A. 2013;110(27):11091-6.

102. Yang H, Yao F, Davis PF, Tan ST, Hall SRR. CD73, Tumor Plasticity and Immune Evasion in Solid Cancers. Cancers (Basel). 2021;13(2).

103. Hu G, Cheng P, Pan J, Wang S, Ding Q, Jiang Z, et al. An IL6-Adenosine Positive Feedback Loop between CD73(+) γδTregs and CAFs Promotes Tumor Progression in Human Breast Cancer. Cancer Immunol Res. 2020;8(10):1273-86.

104. Ren ZH, Lin CZ, Cao W, Yang R, Lu W, Liu ZQ, et al. CD73 is associated with poor prognosis in HNSCC. Oncotarget. 2016;7(38):61690-702.

105. Reinhardt J, Landsberg J, Schmid-Burgk JL, Ramis BB, Bald T, Glodde N, et al. MAPK Signaling and Inflammation Link Melanoma Phenotype Switching to Induction of CD73 during Immunotherapy. Cancer Res. 2017;77(17):4697-709.

106. Koszałka P, Gołuńska M, Urban A, Stasiłojć G, Stanisławowski M, Majewski M, et al. Specific Activation of A3, A2A and A1 Adenosine Receptors in CD73-Knockout Mice Affects B16F10 Melanoma Growth, Neovascularization, Angiogenesis and Macrophage Infiltration. PLoS One. 2016;11(3):e0151420.

107. Sorrentino C, Miele L, Porta A, Pinto A, Morello S. Myeloid-derived suppressor cells contribute to A2B adenosine receptor-induced VEGF production and angiogenesis in a mouse melanoma model. Oncotarget. 2015;6(29):27478-89.

108. Iannone R, Miele L, Maiolino P, Pinto A, Morello S. Blockade of A2b adenosine receptor reduces tumor growth and immune suppression mediated by myeloid-derived suppressor cells in a mouse model of melanoma. Neoplasia. 2013;15(12):1400-9.

109. Merighi S, Benini A, Mirandola P, Gessi S, Varani K, Leung E, et al. A3 adenosine receptors modulate hypoxia-inducible factor-1alpha expression in human A375 melanoma cells. Neoplasia. 2005;7(10):894-903.

110. Sorin M, Rezanejad M, Karimi E, Fiset B, Desharnais L, Perus LJM, et al. Single-cell spatial landscapes of the lung tumour immune microenvironment. Nature. 2023;614(7948):548-54.

111. Keren L, Bosse M, Marquez D, Angoshtari R, Jain S, Varma S, et al. A Structured Tumor-Immune Microenvironment in Triple Negative Breast Cancer Revealed by Multiplexed Ion Beam Imaging. Cell. 2018;174(6):1373-87.e19.

112. Schapiro D, Jackson HW, Raghuraman S, Fischer JR, Zanotelli VRT, Schulz D, et al. histoCAT: analysis of cell phenotypes and interactions in multiplex image cytometry data. Nat Methods. 2017;14(9):873-6.

113. Newman ME. Mixing patterns in networks. Phys Rev E Stat Nonlin Soft Matter Phys. 2003;67(2 Pt 2):026126.

114. Schwartz LH, Litière S, de Vries E, Ford R, Gwyther S, Mandrekar S, et al. RECIST 1.1-Update and clarification: From the RECIST committee. Eur J Cancer. 2016;62:132-7.

115. Smalley I, Chen Z, Phadke M, Li J, Yu X, Wyatt C, et al. Single-Cell Characterization of the Immune Microenvironment of Melanoma Brain and Leptomeningeal Metastases. Clin Cancer Res. 2021;27(14):4109-25.

116. Emri E, Egervari K, Varvolgyi T, Rozsa D, Miko E, Dezso B, et al. Correlation among metallothionein expression, intratumoural macrophage infiltration and the risk of metastasis in human cutaneous malignant melanoma. J Eur Acad Dermatol Venereol. 2013;27(3):e320-7.

117. Phadke M, Ozgun A, Eroglu Z, Smalley KSM. Melanoma brain metastases: Biological basis and novel therapeutic strategies. Exp Dermatol. 2022;31(1):31-42.

118. Weiss SA, Zito C, Tran T, Heishima K, Neumeister V, McGuire J, et al. Melanoma brain metastases have lower T-cell content and microvessel density compared to matched extracranial metastases. J Neurooncol. 2021;152(1):15-25.

119. Herrera-Rios D, Mughal SS, Teuber-Hanselmann S, Pierscianek D, Sucker A, Jansen P, et al. Macrophages/Microglia Represent the Major Source of Indolamine 2,3-Dioxygenase Expression in Melanoma Metastases of the Brain. Front Immunol. 2020;11:120.

120. Unger MS, Schernthaner P, Marschallinger J, Mrowetz H, Aigner L. Microglia prevent peripheral immune cell invasion and promote an anti-inflammatory environment in the brain of APP-PS1 transgenic mice. J Neuroinflammation. 2018;15(1):274.

121. Kluger HM, Zito CR, Barr ML, Baine MK, Chiang VL, Sznol M, et al. Characterization of PD-L1 Expression and Associated T-cell Infiltrates in Metastatic Melanoma Samples from Variable Anatomic Sites. Clin Cancer Res. 2015;21(13):3052-60.

122. Azimi F, Scolyer RA, Rumcheva P, Moncrieff M, Murali R, McCarthy SW, et al. Tumor-infiltrating lymphocyte grade is an independent predictor of sentinel lymph node status and survival in patients with cutaneous melanoma. J Clin Oncol. 2012;30(21):2678-83.

123. Hamid O, Schmidt H, Nissan A, Ridolfi L, Aamdal S, Hansson J, et al. A prospective phase II trial exploring the association between tumor microenvironment biomarkers and clinical activity of ipilimumab in advanced melanoma. J Transl Med. 2011;9:204.

124. Lamba N, Wen PY, Aizer AA. Epidemiology of brain metastases and leptomeningeal disease. Neuro Oncol. 2021;23(9):1447-56.

125. Ahmed MB, Alghamdi AAA, Islam SU, Lee JS, Lee YS. cAMP Signaling in Cancer: A PKA-CREB and EPAC-Centric Approach. Cells. 2022;11(13).

126. Long JS, Crighton D, O'Prey J, Mackay G, Zheng L, Palmer TM, et al. Extracellular adenosine sensing-a metabolic cell death priming mechanism downstream of p53. Mol Cell. 2013;50(3):394-406.

Supplemental Tables and Figures

Supplementary Table S1. Panel of 35 antibodies and the corresponding metal isotopes and clone used.

	Antigen	Metal Conjugate	Clone
Lymphoid Lineage Markers	CD3	170Er	Polyclonal
	CD8a	162Dy	C8/144
	CD4	156Gd	EPR6855
	FoxP3	155Gd	236A/E7
	CD20	161Dy	H1
	CD94	166Er	EPR21003
Myeloid Lineage Markers	CD68	159Tb	KP1
	CD163	147Sm	EDHu-1
	P2Y12	169Tm	Polyclonal
	CD11c	154Sm	EP1347Y
	HLA-DR	174Yb	EPR3692
	CD14	144Nd	SP192
	CD16	142Nd	SP175
	CD117	153Eu	YR145
	MPO	145Nd	EPR20257
Compartment Markers	PanCK	175Lu	AE1+AE3
	PMEL	165Ho	HMB-45
	MelanA	168Er	A103
	CD31	176Yb	JC/70A
	GFAP	141Pr	EP672Y
	DNA1	191 Ir	N/A
	DNA2	193Ir	N/A
	CD45	152Sm	D9M8I
Functional Markers	Ki67	143Nd	B56
	CC3	172Yb	5A1E
	Claudin-5	173Yb	EPR7583
	Ox40L	164Dy	EP1168Y
	MMP9	160Gd	EP1255Y
	MCSF-R	151Eu	SP211
	CTLA-4	158Gd	SP355
	HIF1a	149Sm	EP1215Y
	CD39	167Er	EPR20627
	pERK	171Yb	D13.14.4E
	pSTAT3	163Dy	EP2147Y
	CIRBP	146Nd	EPR18783
	PD-L1 biotin	150Nd	E1L3N
	PD1	148Nd	D4W2J

Supplementary Table S2. Concentration of primary antibody and secondary antibody used for the optimisation of CD73 and A2a.

TMA	Primary Antibody	Dilution	Secondary Antibody	Dilution
Ovarian prostate	CD73 (Abcam, ab91086)	1/200	Rabbit 647 (Invitrogen)	1/400
Ovarian prostate	CD73 (Abcam, ab91086)	1/400	Rabbit 647 (Invitrogen)	1/400
Ovarian prostate	CD73 (Abcam, ab91086)	1/800	Rabbit 647 (Invitrogen)	1/400
Ovarian prostate	A2A 7F6 65-A2	1/50	Mouse IgG1 647 (Invitrogen, A21240)	1/400
Ovarian prostate	A2A 7F6 65-A2	1/100	Mouse IgG1 647 (Invitrogen, A21240)	1/400
Ovarian prostate	A2A 7F6 65-A2	1/200	Mouse IgG1 647 (Invitrogen, A21240)	1/400

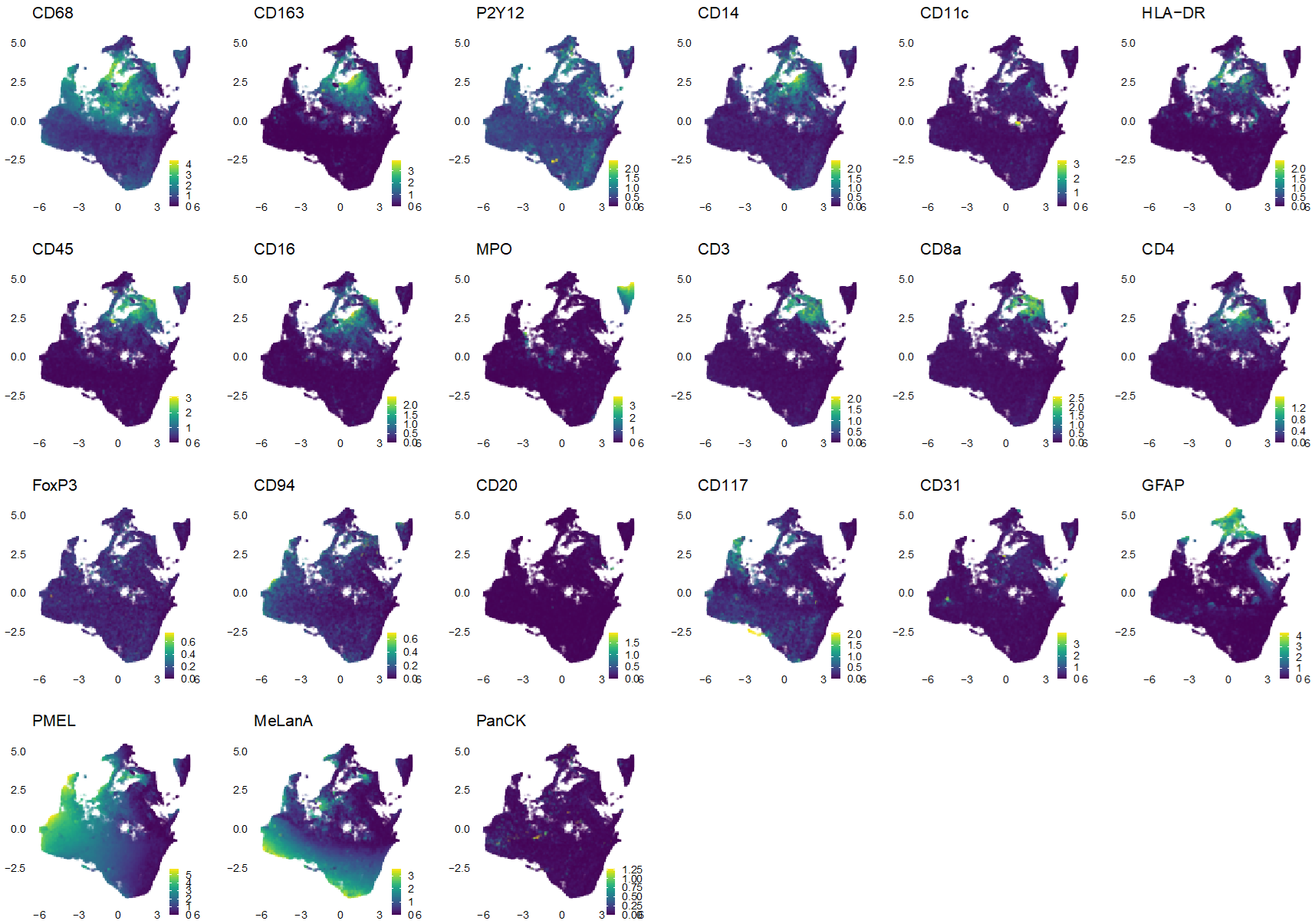

Supplementary Figure S1. Marker intensity overlaid on UMAP projections where points are colored by marker intensity. A threshold at percentile .999 has been used for visualization purposes.

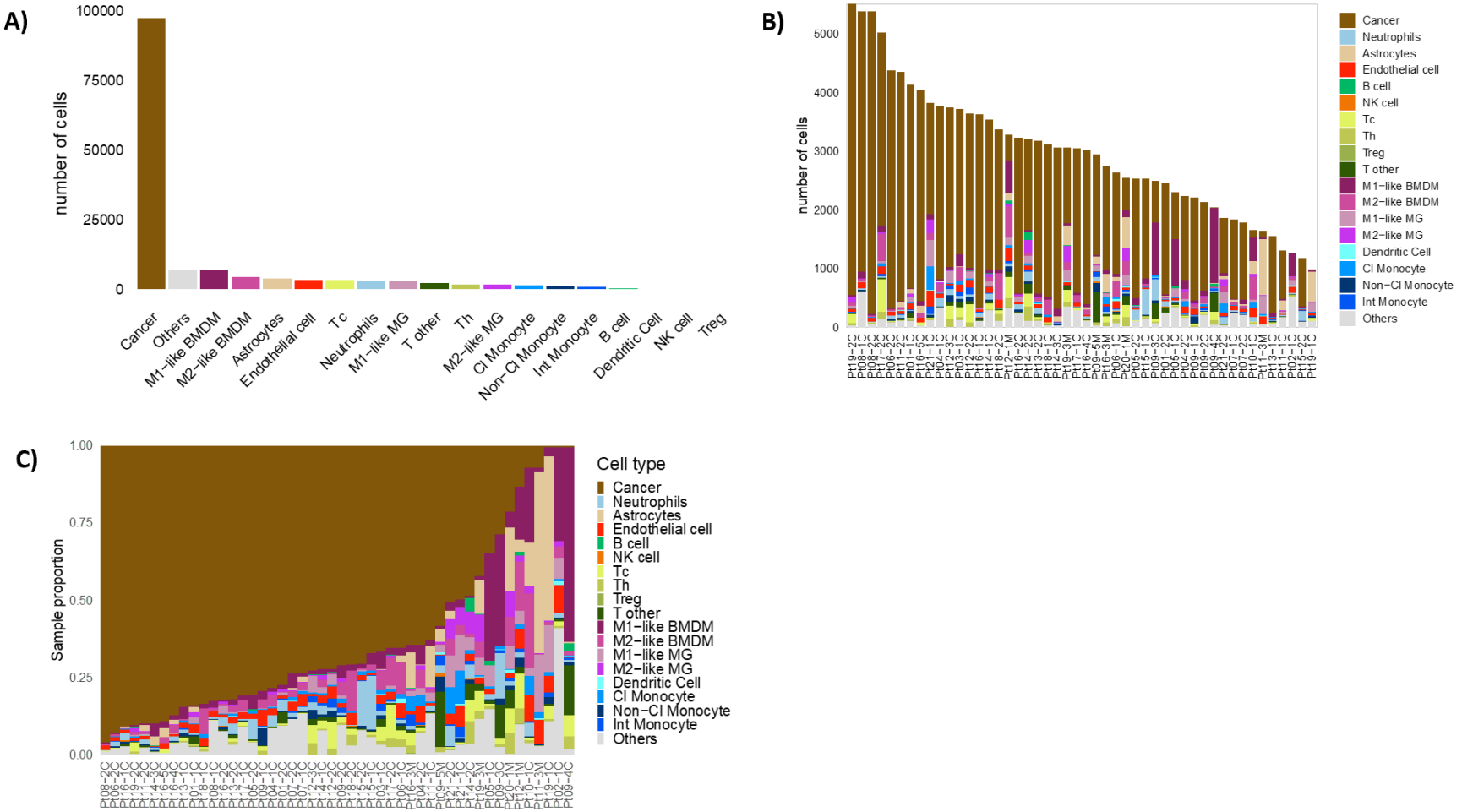

Supplementary Figure S2. A) Total number of cells identified for each cell type. B) Total number of cells identified for each cell type for each patient. C) Stacked bar plot of the proportion of all the different cell types in every sample ordered by increasing proportion of melanoma cells.

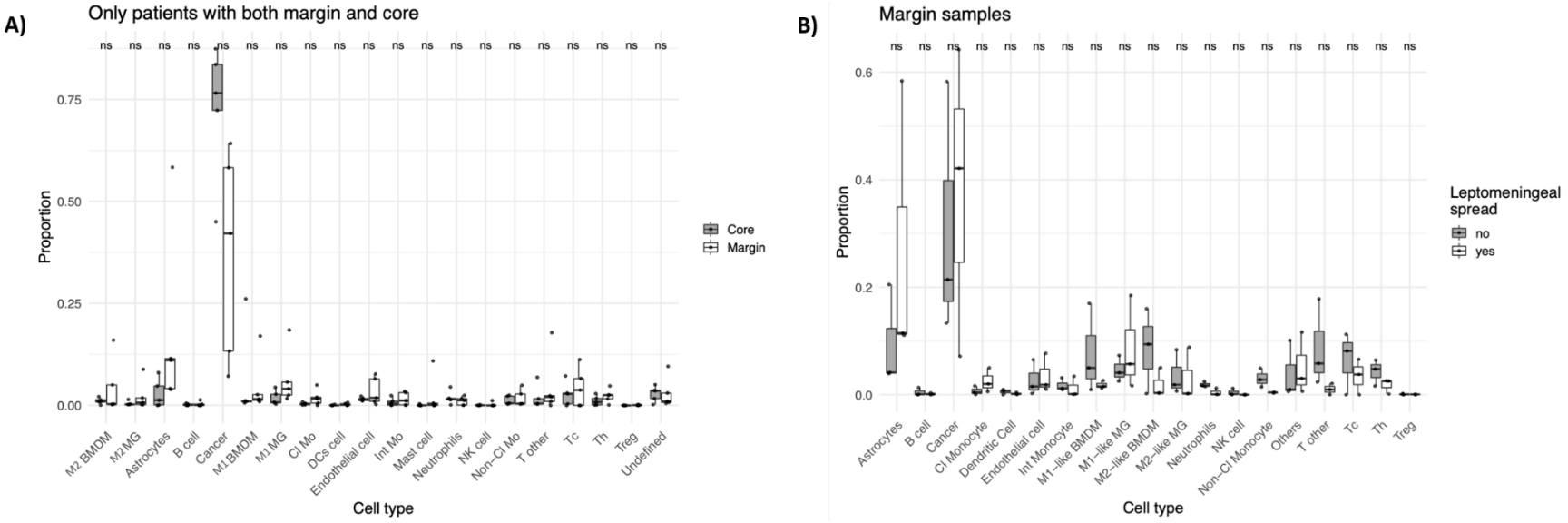

Supplementary Figure S3. Cell type proportion comparisons. Boxplot of distribution of cell type proportions in every sample by comparing A) cores and margins where cores from the same patient have been merged (only patients that have both core and margin samples), B) patients with or without leptomeningeal spread (margin samples only).

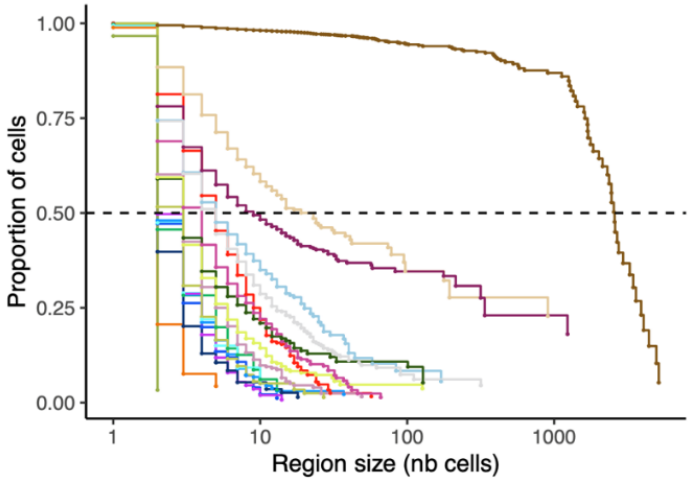

Supplementary Figure S4. Proportion of cells found within region of size.

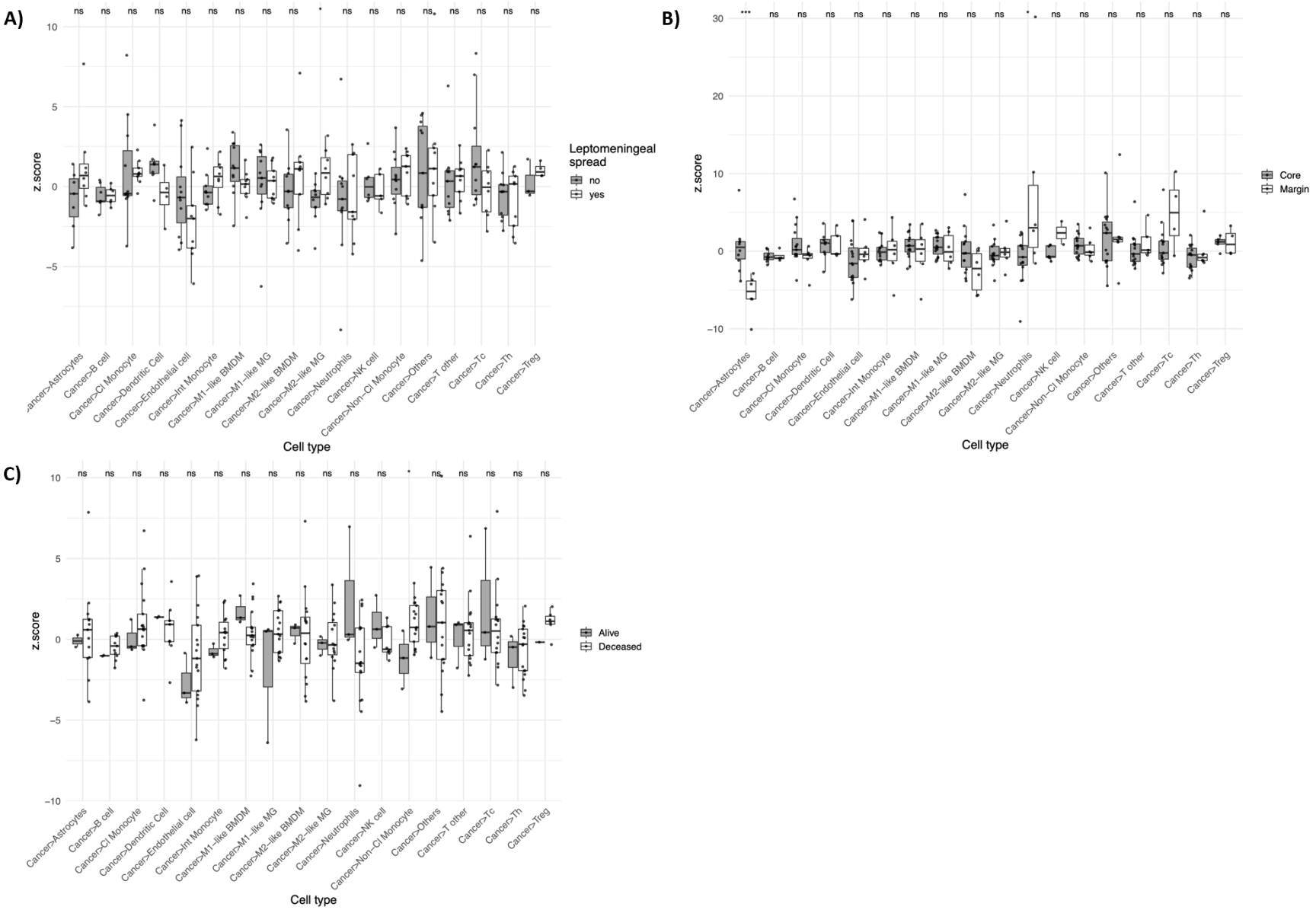

Supplementary Figure S5. Z score of A) Leptomeningeal status, B) core and margin, C) alive and deceased.

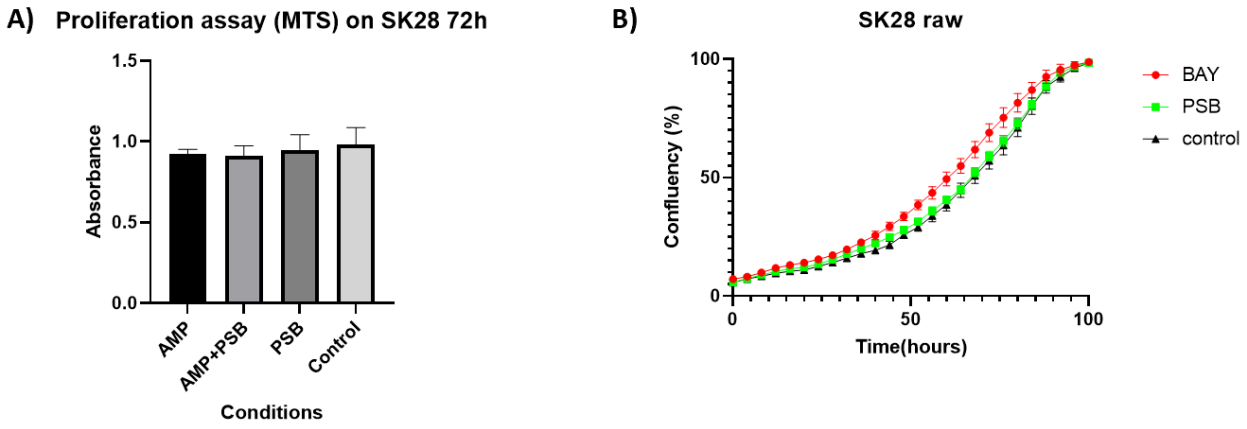

Supplementary Figure S6. Proliferation of SK28 cell line. A) Proliferation assay (MTS) at 72h when adding AMP. B) Proliferation assay when adding BAY and PSB using IncuCyte (p value calculated using the linear portion of each condition).